SCADA Continues to Thrive in the Industrial World Despite the Presence of IoT **p24**

An In-Depth Look at the Essential Parts Needed in Ultra-Low-Noise Synthesizer Design **p44**

Can Self-Interference Cancellation Rescue IoT in the 2.4-GHz Band? **p54**

Microwaves & RF®

YOUR TRUSTED ENGINEERING RESOURCE FOR OVER 50 YEARS

OCTOBER 2019 mwrf.com

MEASURE EVM

Using Modulation Distortion

This novel approach combines a VNA and VSG with a MOD app **p19**

$10.00

Planar Monolithics Industries, Inc.

Broadband Frequency Discriminators

PMI is an industry leader in the design and manufacturing of RF and Microwave Frequency Discriminators offering a robust line of products that range up to 18.0 GHz. A wide selection of standard models with various options are available including Digital or Analog output. Visit our website for a full listing of Frequency Discriminators.
https://www.pmi-rf.com/categories/frequency-discriminators


DFD-2G18G-5512


FD-30M-6M-1515


FD-70M-50M-1212


FD-1G-500M-55-SFF


FD-0518-10-118

PMI Model No.	Frequency Range (GHz)	Output	Rise Time	Input Dynamic Range (dBm)	Input VSWR	DC Voltage & Current (Max)	Size Connector
DFD-2G18G-5512 (Digital) https://www.pmi-rf.com/product-details/dfd-2g18g-5512	2 - 18	1 MHz/bit	50 ns	-50 to +15	2.0:1	+5 VDC @ 1480 mA, -5 VDC @ 30 mA, +12 VDC @ 800 mA	5.98" x 5.79" x 1.28" SMA Female
FD-30M-6M-1515 (Analog) https://www.pmi-rf.com/product-details/fd-30m-6m-1515	30 MHz	1000 mV/ MHz ± 5% into 50 Ohms	120 ns	-10 to 0	1.09:1	+15 VDC @ 79 mA, -15 VDC @ 51 mA	4.625" x 1.5" x 0.47" SMA Female
FD-70M-50M-1212 (Analog) https://www.pmi-rf.com/product-details/fd-70m-50m-1212	70 MHz	100 mV/ MHz ± 5% into 93 ohms	50 ns	-10 to 0	1.1:1	+12 VDC @ 77 mA, -12 VDC @ 48 mA	4.625" x 1.5" x 0.47" SMA Female
FD-1G-500M-55-SFF (Analog) https://www.pmi-rf.com/product-details/fd-1g-500m-55-sff	1	10 mV/MHz Typ into 93 Ohms	10 ns	-10 to 0	2.0:1	+5 VDC @ 25 mA, -5 VDC @ 70 mA	2.5" x 1.0" x 0.4" SMA Female
FD-0518-10-118 (Analog) https://www.pmi-rf.com/product-details/fd-0518-10-118	1 - 18	75 – 450 mV/GHz	20 ns	+10 ± 0.1	2.0:1	+15 VDC @ 875 mA, -15 VDC @ 150 mA	8.5" x 5.0" x 3.75" SMA Female
FD-0518-10-2G4G (Analog) https://www.pmi-rf.com/product-details/fd-0518-10-2g4g	2 - 4	1 V/GHz	20 ns	+10 ± 0.1	1.5:1	+15 VDC @ +75 mA, -15 VDC @ -75 mA	2.0" x 1.8" x 0.5" SMA Female
FD-0518-10-3D1G3D5G (Analog) https://www.pmi-rf.com/product-details/fd-0518-10-3d1g3d5g	3.1 - 3.5	50 mV/GHz	10 ns	+10 ± 0.1	1.68:1	+15 VDC @ +15 mA, -15 VDC @ -12 mA	2.0" x 1.8" x 0.5" SMA Female
FD-0518-10-48-OPT3R5G5R5G (Analog) https://www.pmi-rf.com/product-details/fd-0518-10-48-opt3r5g5r5g	3.5 - 5.5	1 V/GHz	20 ns	+10 ± 0.1	1.35:1	-+15 VDC @ +38 mA, -15 VDC @ -10 mA	2.0" x 1.8" x 0.5" SMA Female
FD-0518-10-618 (Analog) https://www.pmi-rf.com/product-details/fd-0518-10-618	6 - 18	50 mV/GHz	20 ns	+10 ± 0.1	1.5:1	+15 VDC @ +50 mA, -15 VDC @ -50 mA	2.0" x 1.8" x 0.5" SMA Female
FD-0518-10-812 (Analog) https://www.pmi-rf.com/product-details/fd-0518-10-812	8 - 12	50 mV/GHz	5 ns	+10 ± 0.1	1.44:1	+15 VDC @ +11 mA, -15 VDC @ -11 mA	2.0" x 1.8" x 0.5" SMA Female
FD-0518-10-1218 (Analog) https://www.pmi-rf.com/product-details/fd-0518-10-1218	12 - 18	50 mV/GHz	20 ns	+10 ± 0.1	1.5:1	+15 VDC @ 58 mA, -15 VDC @ 12 mA	2.0" x 1.8" x 0.5" SMA Female


FD-0518-10-2G4G


FD-0518-10-3D1G3D5G


FD-0518-10-48-OPT3R5G5R5G


FD-0518-10-618


FD-0518-10-812


FD-0518-10-1218

56th Annual AOC International Symposium & Convention
October 28 - 30, 2019
Renaissance Downtown Washington DC & Convention Center, Washington, DC
Booth # 907
https://www.crows.org/mpage/2019home

West Coast Operation:
4921 Robert J. Mathews Pkwy, Suite 1
El Dorado Hills, CA 95762 USA
Tel: 916-542-1401, Fax: 916-265-2597

East Coast Operation:
7311-F Grove Road
Frederick, MD 21704 USA
Tel: 301-662-5019, Fax: 301-662-1731

sales@pmi-rf.com • www.pmi-rf.com

ISO 9001-2015 REGISTERED

- **Amplifiers – Solid State**
- **Attenuators – Variable/ Programmable**
- **Couplers (Quadrature, 180° & Directional)**
- **Detectors – RF/Microwave**
- **DLVAs, ERDLVAs & SDLVAs**
- **DTOs, VCOs, PLO, DROs, & Frequency Synthesizers**
- **Filters & Switched Filter Banks**
- **Form, Fit, Functional Products & Services**
- **Frequency Discriminators & IFMs**
- **Integrated MIC/MMIC Assemblies (IMAs)**
- **IQ Vector Modulators**
- **Limiters – RF/Microwave**
- **Log Amplifiers**
- **Millimeter Wave Components (Up to 50 GHz)**
- **Miscellaneous Products**
- **Monopulse Comparators**
- **Multifunction Integrated Assemblies (MIAs)**
- **Phase Shifters & Bi-Phase Modulators**
- **Power Dividers/Combiners (Passive & Active)**
- **Pulse Modulators (SPST)**
- **Rack & Chassis Mount Products**
- **Receiver Front Ends & Transceivers**
- **SDLVAs, ERDLVAs & DLVAs**
- **Single Side Band Modulators**
- **SMT & QFN Products**
- **Switch Matrices**
- **Switched Filter Banks**
- **Switches – Solid State**
- **Systems - Radar Sense & Avoid**
- **Systems – Fly Eye Radars**
- **Threshold Detectors**
- **USB Products**


NATIONAL INSTRUMENTS
TOMORROW'S DESIGNS REQUIRE
SMARTER
SOFTWARE TODAY
AWR
NI AWR Design Environment software provides a seamless platform for developing next-generation wireless electronics and communications systems, from concept to product. Its powerful interface, integrated system, circuit, and electromagnetic simulation technologies, and design flow automation ensures your design success.
Visit awr.com/smarterdesign to learn more.
©2019 National Instruments Corporation. All rights reserved. AWR, AWR Design Environment, National Instruments, and NI are trademarks of National Instruments. Other product and company names listed are trademarks or trade names of their respective companies.

IN THIS ISSUE

FEATURES

19

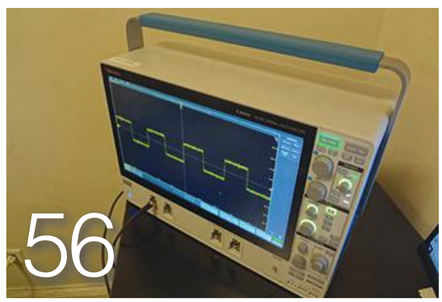

NEWS & COLUMNS

PRODUCTS & TECHNOLOGY

JOIN US ONLINE

follow us @MicrowavesRF

become a fan at facebook.com/microwavesRF

62

ON MICROWAVES&RF.COM

Materials Provide Connections and Protection

Advanced materials enable the creation of selectively permeable fabrics to block the flow of dangerous chemicals in the warehouse or on the battlefield.

https://www.mwrf.com/defense/materials-provide-connections-and-protection

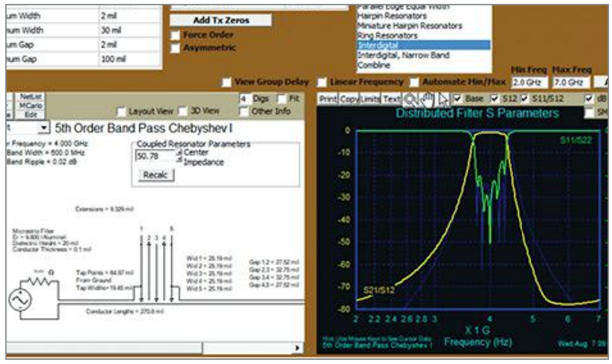

Workflow Carves a Path to Effective Filter Design

A simulation-based filter design example demonstrates a semi-automated workflow that can help designers achieve first-pass success.

https://www.mwrf.com/software/workflow-carves-path-effective-filter-design

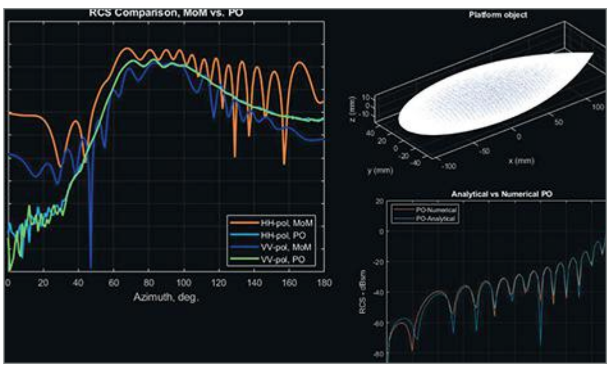

Algorithms to Antenna: Benchmarking Radar Cross Section

Following up our recent blog on methods that tackle radar cross section of simple point targets and extended targets, this edition zeros in on benchmarks for RCS.

https://www.mwrf.com/systems/algorithms-antenna-benchmarking-radar-cross-section

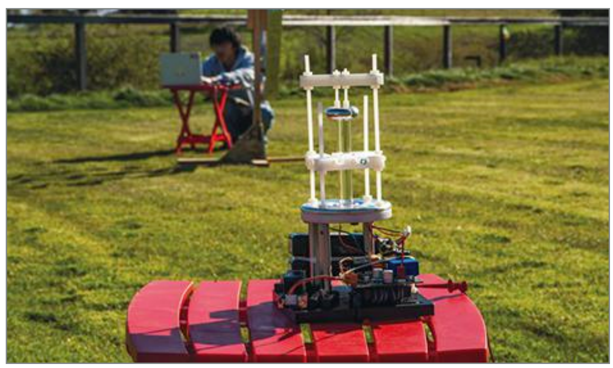

Piezo-Based Approach Dramatically Shrinks VLF Antennas

A research team developed VLF antennas using piezoelectric material and principles, resulting in an antenna that's far smaller than metal antennas, thus overcoming a major impediment to VLF links.

https://www.mwrf.com/components/piezo-based-approach-dramatically-shrinks-vlf-antennas

join us online

twitter.com/MicrowavesRF facebook.com/microwavesrf

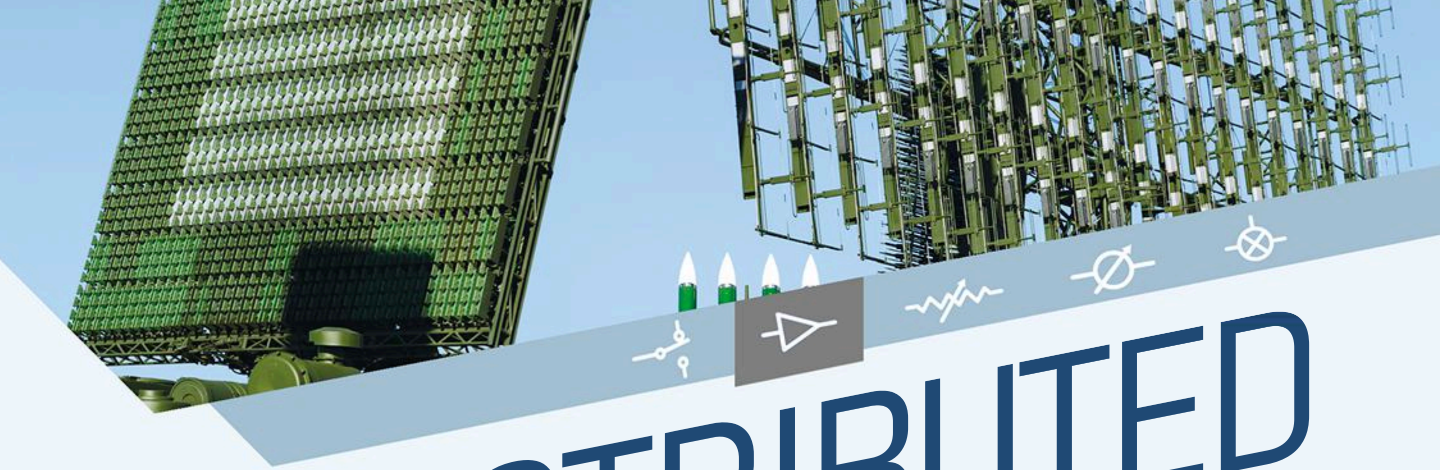

GaAs

DISTRIBUTED AMPLIFIERS

WIDE BANDWIDTH DC - 40 GHz

High Frequency Surface Mount Packaging Available

*Custom MMIC now offers select products, over 20 GHz, in plastic surface mount air-cavity QFN packages. This new "K" series package maintains performance similar to die level and can be tested with our easy to use **ev**aluation boards. Order one today!*

CMD242K4

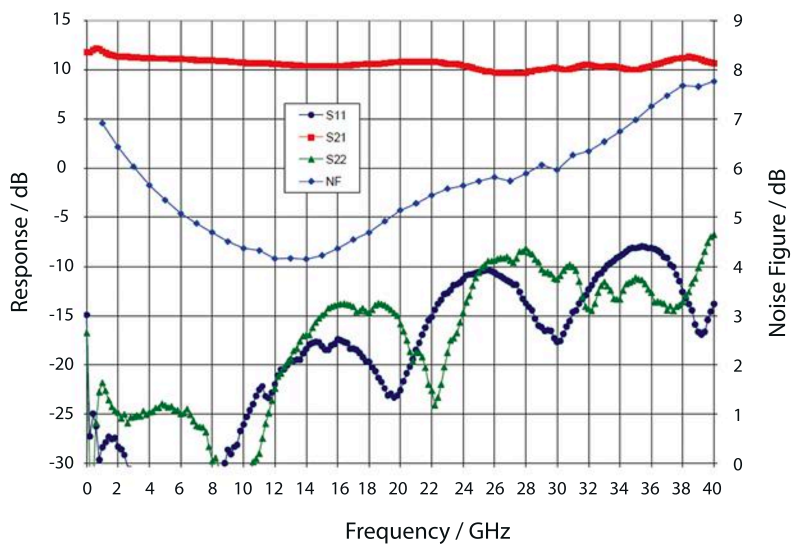

Delivering performance without compromise

The CMD242K4 is a wideband GaAs Distributed Amplifier that operates from DC to 40 GHz, providing customers with a broad frequency range of operation and industry leading performance making this MMIC perfect for EW, Test/Instrumentation and a host of other millimeter wave applications.

Where can we take you next?

Custom MMIC
CustomMMIC.com

Editorial

CHRIS DeMARTINO | Editor
chris.demartino@informa.com

Has Simulation Software Made Us SMARTER?

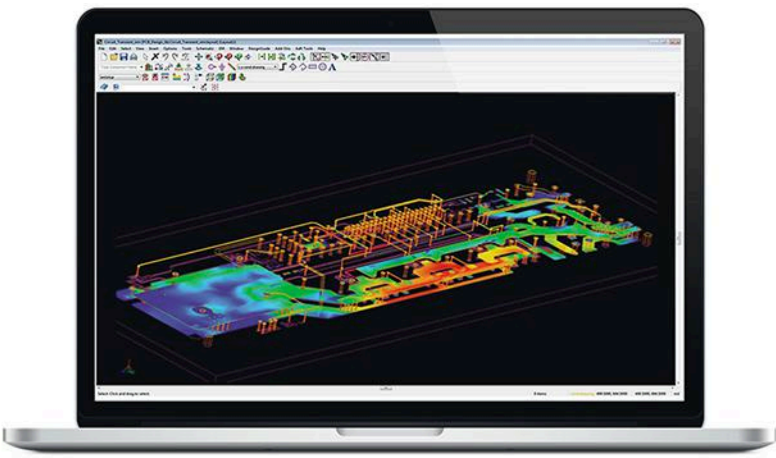

One cannot question the advanced capabilities of modern simulation software tools, but how is that affecting the next generation of engineers?

Today's high-frequency simulation software tools provide engineers with advanced capabilities that were simply not available in years past. These tools are obviously a tremendous benefit to today's engineers tasked with solving complex problems. So, one could argue that today's engineers have a clear advantage over previous generations of engineers who did not have such sophisticated tools at their disposal during the design process.

However, with simulation software reaching such an advanced level, one could speculate whether these tools are having a positive impact on younger engineers. Simply put, have the capabilities of today's simulation software tools prevented younger engineers from learning theoretical concepts?

How-Siang Yap, Genesys product manager at Keysight Technologies *(www.keysight.com)*, responded, "Initially, engineers might be tempted to rely on brute-force optimization or automatic circuit synthesis to do their jobs. But that's only until they realize the truth about 'garbage in, garbage out,' in which there's no replacement of learning the theoretical concepts behind good engineering. Advanced

(Continued on page 8)

(Continued from page 7)

Do younger engineers have an easier path to success thanks to the capabilities of today's simulation software tools?

simulation capabilities enable them to expand the application of fundamental theoretical concepts to tackle problems that are many orders of magnitude more complex than problems that can be solved manually."

Following on that, another question could be: Compared to past generations of engineers, do younger engineers have an easier path to success thanks to the capabilities of today's simulation software tools? Yap answered with, "Yes, definitely. Today's simulation tools enable fast exploration of multiple design options to determine the optimal combination of performance, size, and cost that can be accurately realized in actual hardware with minimal or no iterations. These simulated design explorations replace traditional 'cut-and-try' techniques, enabling younger engineers to gain design and troubleshooting experience much faster to tackle ever more complex designs."

One additional point, brought up by an engineer at a recent conference, is that as a byproduct of advanced simulation software tools, engineers are now required to produce more (at least in his case). So, in that sense, simulation software hasn't necessarily made the job of an engineer easier, but rather it's resulted in even more work.

No matter where you stand in terms of this debate, there's no doubt that simulation software has had a significant impact on this industry. And you can bet that the companies providing these tools will have more tricks to unveil in the future. mw

Microwaves&RF OCTOBER 2019

EDITORIAL

GROUP CONTENT DIRECTOR: **KAREN FIELD** karen.field@informa.com
SENIOR CONTENT DIRECTOR: **BILL WONG** bill.wong@informa.com
EDITOR: **CHRIS DeMARTINO** chris.demartino@informa.com
SENIOR STAFF WRITER: **JAMES MORRA** james.morra@informa.com
TECHNICAL EDITOR: **JACK BROWNE** jack.browne@informa.com
ASSOCIATE EDITOR/COMMUNITY MANAGER: **ROGER ENGELKE** roger.engelke@informa.com

ART DEPARTMENT

GROUP DESIGN DIRECTOR: **ANTHONY VITOLO** tony.vitolo@informa.com
CONTENT DESIGN SPECIALIST: **JOCELYN HARTZOG** jocelyn.hartzog@informa.com
CONTENT & DESIGN PRODUCTION MANAGER: **JULIE JANTZER-WARD** julie.jantzer-ward@informa.com

PRODUCTION

GROUP PRODUCTION MANAGER: **GREG ARAUJO** greg.araujo@informa.com
PRODUCTION MANAGER: **VICKI McCARTY** vicki.mccarty@informa.com

AUDIENCE MARKETING

USER MARKETING MANAGER: **DEBBIE BRADY** debbie.brady@informa.com

FREE SUBSCRIPTION / STATUS OF SUBSCRIPTION / ADDRESS CHANGE/ MISSING BACK ISSUES:
OMEDA **T** | 847.513.6022 **TOLL FREE** | 866.505.7173

SALES & MARKETING

MANAGING DIRECTOR: **TRACY SMITH** **T** | 913.967.1324 **F** | 913.514.6881 tracy.smith@informa.com
REGIONAL SALES REPRESENTATIVES:
AZ, NM, TX: **GREGORY MONTGOMERY** **T** | 480.254.5540 gregory.montgomery@informa.com
AK, NORTHERN CA, OR, WA, WESTERN CANADA: **STUART BOWEN** **T** | 425.681.4395 stuart.bowen@informa.com
AL, AR, SOUTHERN CA, CO, FL, GA, HI, IA, ID, IL, IN, KS, KY, LA, MI, MN, MO, MS, MT, NC, ND, NE, NV, OH, OK, SC, SD, TN, UT, VA, WI, WV, WY, CENTRAL CANADA: **JAMIE ALLEN** **T** | 415.608.1959 **F** | 913.514.3667 jamie.allen@informa.com
CT, DE, MA, MD, ME, NH, NJ, NY, PA, RI, VT, EASTERN CANADA:
ELIZABETH ELDRIDGE **T** | 917.789.3012 elizabeth.eldridge@informa.com

INTERNATIONAL SALES:
GERMANY, AUSTRIA, SWITZERLAND: **CHRISTIAN HOELSCHER** **T** | 011.49.89.95002778
christian.hoelscher@husonmedia.com
BELGIUM, NETHERLANDS, LUXEMBURG, UNITED KINGDOM, SCANDINAVIA, FRANCE, SPAIN, PORTUGAL:
JAMES RHOADES-BROWN **T** | +011 44 1932 564999 **M** | +011 44 1932 564998 james.rhoadesbrown@husonmedia.co.uk
ITALY: **DIEGO CASIRAGHI** diego@casiraghi-adv.com
PAN-ASIA: **HELEN LAI** **T** | 886 2-2727 7799 helen@twoway-com.com
PAN-ASIA: **CHARLES LIU** **T** | 886 2-2727 7799 liu@twoway-com.com

PLEASE SEND INSERTION ORDERS TO: orders@informa.com
INFORMA REPRINTS: **WRIGHT'S MEDIA** **T** | 877.652.5295
LIST RENTALS/ SMARTREACH CLIENT SERVICES MANAGER: **MARY RALICKI** **T** | 212.204.4284
mary.ralicki@informa.com

DIGITAL

GROUP DIGITAL DIRECTOR: **RYAN MALEC** ryan.malec@informa.com

DESIGN ENGINEERING & SOURCING GROUP

GROUP CONTENT DIRECTOR: **KAREN FIELD** karen.field@informa.com
VP OF MARKETING: **JACQUIE NIEMIEC** jacquie.niemiec@informa.com

INFORMA MEDIA INC.

605 THIRD AVENUE
NEW YORK, NY 10158 USA **T** | 212.204.4200

informa

Electronic Design | Machine Design | Microwaves & RF | Source ESB | Hydraulics & Pneumatics | Global Purchasing | Distribution Resource | Power Electronics | Defense Electronics

News

5G COULD RESTART GROWTH in Smartphone Market by 2020

Shipments of 5G smartphones will surge to more than 100 million units by the end of 2020 as the coverage of 5G networks grows and the premium prices of today's handsets come down, according to a report by International Data Corporation. IDC said that next year 5G handsets could account for close to 10% of global volumes, which have been hammered in recent years by consumers taking longer and longer to upgrade to new models.

The global rollout of 5G technology could turn things around in the mature smartphone market, which has been struggling to return to growth over roughly the last three years. In its latest forecast, IDC said shipments of 5G smartphones could reach 9% market share by the end of 2020, with global shipments skyrocketing to 123.5 million units next year. IDC sees shipments of 5G-enabled handsets rising sharply to 28% of global phone volumes by the end of 2023.

2G, 3G, 4G and 5G smartphones shipments are set to decline slightly in the second half of the year even as OEMs push to clear out inventory ahead of 5G handset production ramping up in 2020, IDC said. Shipments are set to shrink by more than 2% year-over-year in 2019, marking three straight years of declines. IDC expects to see 1.6% growth in shipments next year as consumers shell out for smartphones that can connect to 5G networks being rolled out globally.

Sales of early 5G smartphones have been hampered in large part by prices that often top $1,000. Qualcomm is the primary provider of modem chips for the vast majority of smartphones that can hook to 5G networks, which are designed to transfer data 10 to 100 times faster than current 4G LTE technology. The San Diego, California-based company is selling modems to Oppo, Vivo, Xiaomi, LG and Samsung, which also plans to sell phones with its own integrated 5G SoCs.

Industry analysts say 5G smartphone prices will start to come down in 2020. Qualcomm plans to add its 5G modems to its mid-range Snapdragon Series 6 and Series 7 apps processors, which are today slapped inside smartphones that cost from $200 to $400. Adding 5G technology to more affordable chips could help more than 2 billion smartphones to upgrade to new models, Qualcomm said. The 5G Snapdragon 7 Series SoCs are due out in phones by early 2020.

IDC said it cut the projected average selling prices of 5G smartphones in its latest forecast, particularly in China. Ryan Reith, vice president of IDC's worldwide mobile device tracker, said mid-range 5G handsets will start shipping in 2020 for sub-6 GHz bands—the frequency range favored in China and Europe for early 5G deployments. Baseband modems that can only access the sub-6 GHz frequencies generally cost less than chips that also work with millimeter wave networks.

"To be clear, we don't think 5G will be the savior in smartphones, but we do see it as a critical evolution in mobile technology," Reith said in a statement. "We expect the 5G ramp on smartphones to be more subtle than what we saw with 4G, but that is primarily because we are in a much different market today. The biggest difference is the level of penetration we are at now." ■

SETTING THE STAGE for mmWave 5G

IN A RECENT ANNOUNCEMENT, Analog Devices (ADI) *(www.analog.com)* unveiled a highly integrated solution that's intended to accelerate millimeter-wave (mmWave) 5G wireless network infrastructure. According to ADI, this solution "offers the highest available level of integration to reduce design requirements and complexity in the next generation of cellular network infrastructure."

The ADMV1017 mmWave up/downconverter covers a frequency range of 24 to 29.5 GHz.

Before discussing the new solution, it's worthwhile to get some insight from Kerem Ok, product line director at ADI. Ok recently weighed in on the mmWave 5G landscape and explained how that's affecting ADI. "We're seeing that there's a concrete push to roll out mmWave 5G, primarily in the U.S. and southeast Asia with the expectation that Europe is going to catch up in the next several years. Our customers are asking us for specific power-efficient, low-cost, high-density offerings that allow them to address this 5G market in which the focus is enabling multi-Gb/s wireless communications for access, backhaul, and fronthaul."

Ok continued, "Traditionally, wireless access has mostly been associated with sub-6-GHz frequencies. It's been believed that it's not possible to deliver information to the consumer at 28 and 39 GHz because of various propagation challenges, atmospheric absorption, requirements for line of sight, etc. However, some of these issues are increasingly being resolved by beamforming. Several different techniques that are part of 5G allow end customers to deliver high-quality data at these bands that were once considered niche."

ADI'S NEW mmWAVE 5G SOLUTION

Everything that Ok mentioned sets the stage for ADI's new mmWave 5G solution, which includes the 16-channel ADMV4821 dual-polarization beamformer, the 16-channel ADMV4801 single-polarization beamformer, and the ADMV1017 mmWave up/downconverter *(see figure)*. All products cover a frequency range of 24 to 29.5 GHz. Combining the ADMV4821/ADMV4801 beamformer with the ADMV1017 up/downconverter results in a 3GPP-compliant 5G New Radio (NR) mmWave front-end solution that addresses the n257, n258, and n261 bands.

According to Ok, "the solution is unique because it's the first wideband 16-channel commercially available dual-/single-polarization beamformer that's 3GPP compliant across the n257, n258, and n261 bands." Ok also noted that the solution offers "industry-leading output power, industry-leading noise figure, and several different flexible IP cores that allow ADI to customize the solutions with different integration levels at both the 24- to 28-GHz and 39-GHz bands."

Ok continued, "One added layer is that our mmWave beams-to-bits capability with enabling algorithms really sets us apart. We are able to add algorithms, addressing array calibration and digital predistortion (DPD), around some of the hardware that we're offering to really push the envelope in terms of performance levels."

The 16-channel ADMV4801 single-polarization beamformer and 16-channel ADMV4821 dual-polarization beamformer feature high-resolution vector modulators for phase control. They both also incorporate high-resolution digital-gain amplifiers (DGAs) for amplitude control.

The ADMV1017 mmWave up/down converter offers 1.5 GHz of bandwidth. It has two upconversion modes along with two downconversion modes. ■

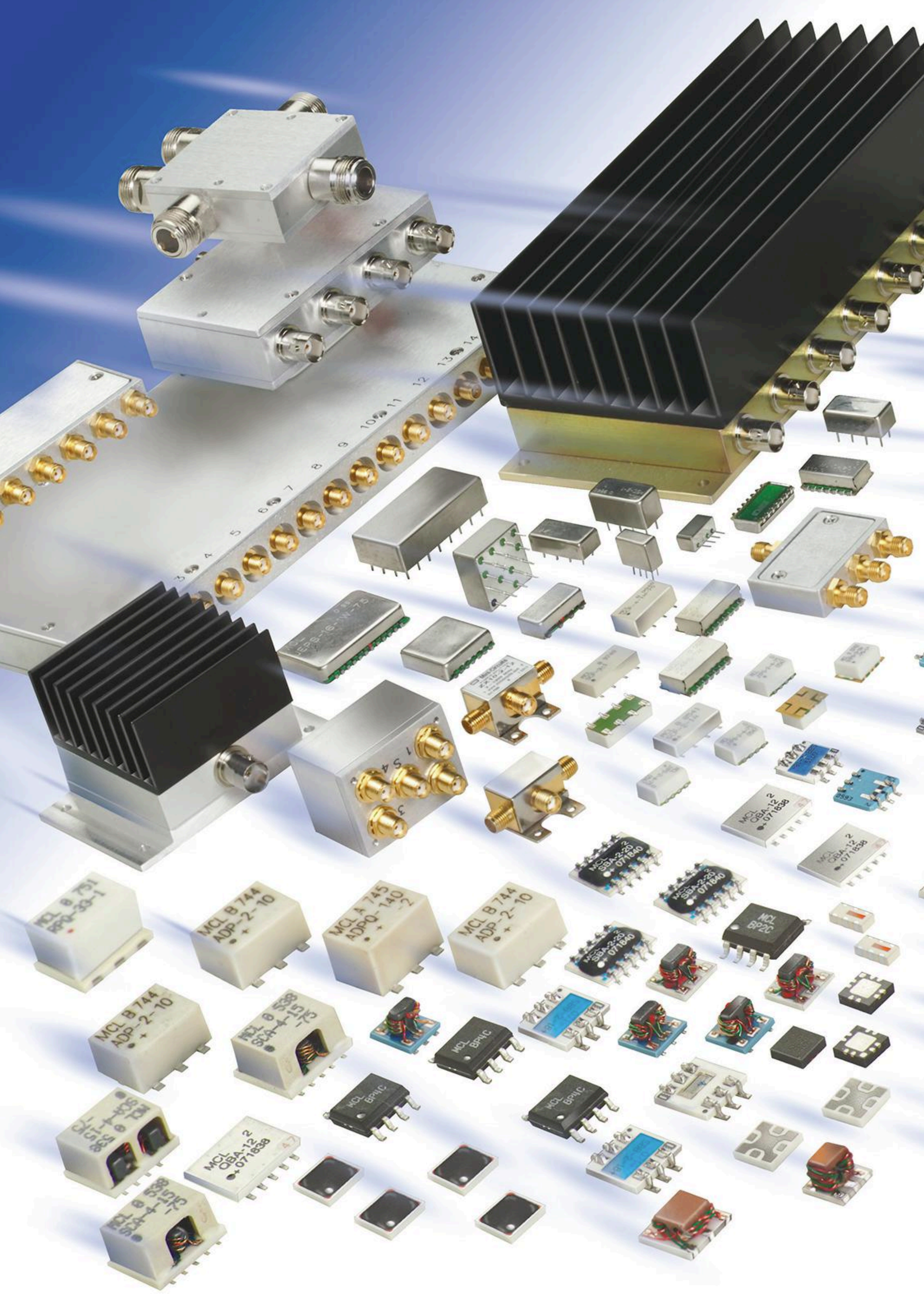

MCL B 744 ADP-2-10
MCL A 745 ADPQ-140-2
MCL B 744 ADP-2-10
MCL B 744 ADP-2-10
MCL B 538 SCA-4-15-75
MCL QBA-12 071838
MCL SBA-2-20 071840
MCL BP2C
MCL BP4C

QUALCOMM BUYS TDK'S STAKE in RF Business for $1.15 Billion

QUALCOMM IS SPENDING $1.15 billion to buy out the radio-frequency chip business it operated with TDK, looking to supply a broader range of components for 5G handsets and other devices. The San Diego, Calif.-based company is aiming to make more money per 5G smartphone by selling a more complete range of chips and packaging them into the radio-frequency front end (RFFE) that connects the core cellular modem to the antenna.

Qualcomm, which has been grappling with a global slowdown in smartphone sales, partnered with TDK to launch RF360 Holdings in 2016. The venture focused on developing SAW, BAW, TC-SAW, and other RF filters and modules that can separate out the specific frequency bands used by 2G, 3G, 4G, and 5G technologies. Qualcomm's stake in the partnership was 51% while TDK owned 49%. By 2017, the joint venture had around 4,000 employees.

Qualcomm has shelled out $3.1 billion over roughly the last three years to cover the transfer of TDK's technology and patents, payouts based on the venture's sales and other investments. The company is trying to gain ground on Broadcom, Qorvo, Skyworks, and other major players in the market for chips slipping inside the radio frequency front end. From 2017 to 2023, the market will more than double to $35 billion, according to Yole Développement.

Qualcomm has long led the roughly $20 billion market for modem chips capable of handling 2G, 3G, and 4G. But in recent years, it has started selling more of the RF chips surrounding its baseband modems. That includes power amplifiers, switches, antenna tuners, filters, envelope trackers, and other parts packaged into modules.

Qualcomm is also selling end-to-end systems—or what it calls modem-to-antenna solutions—for tapping 5G tech. Customers will be able to buy packages of its Snapdragon SoCs, 5G modems, RF transceivers, RF front ends, and antenna modules for sub-6-GHz and millimeter waves that are smaller and highly integrated. That will lead to more lower-power 5G handsets, Qualcomm said.

In August, the company rolled out its latest RFFE for its second-gen X55 5G modem, which also contains all of the components for 2G, 3G, and 4G, but not the core CPU and GPU. The RFFE module is designed to handle both sub-6-GHz and millimeter wave. That could reduce overall costs for handset vendors, which have had to buy separate 5G modems, RFFE modules, and RF transceivers to support both 4G LTE and 5G NR. ■

Transient Immunity Testers from AVTECH

The Avtech AVRQ series of high-voltage, high-speed pulse generators is ideal for testing the common-mode transient immunity (CMTI) of next-generation optocouplers, isolated gate drivers, and other semiconductors.

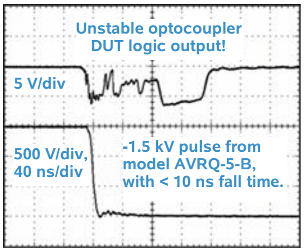

- Kilovolt amplitudes (±1, ±1.5, -2 kV)
- Transition times down to 10 ns, dV/dt rates up to 120 kV/us
- Switchable daughterboards to handle a variety of DUT package styles
- GPIB, RS-232 ports standard
- Ethernet / VXI optional

AVTECH
Nanosecond Electronics
Since 1975

Pricing, manuals, datasheets and test results at:
http://www.avtechpulse.com/semiconductor

30, 50 and 100 Volt Lab Pulsers

Avtech offers an extensive series of user-friendly 30, 50 & 100 Volt general-purpose lab pulsers. We can provide an alternative for the discontinued Agilent 8114A or HP214!

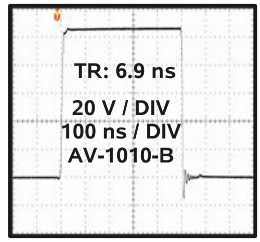

Model AV-1015-B:	**50 Volts, 10 MHz**
Model AV-1010-B:	**100 Volts, 1 MHz, 25 ns to 10 ms, 10 ns rise time**
Model AV-1011B1-B:	**100 Volts, 2 ns rise time**
Model AV-1011B3-B:	**30 Volts, 0.5 ns rise time**

Variable baseline and burst mode options and output currents to 8 Amps with accessory transformers.

AVTECH
Nanosecond Electronics
Since 1975

Pricing, manuals, datasheets and test results at:
http://www.avtechpulse.com/general

Nanosecond Laser Diode Drivers With Butterfly Diode Sockets

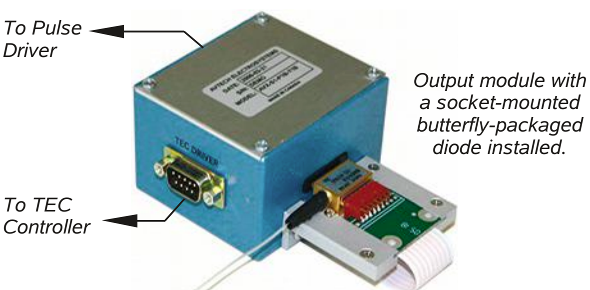

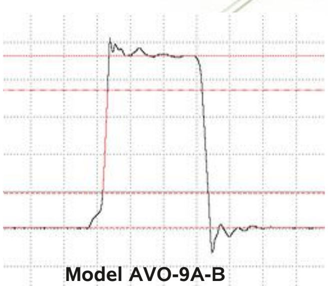

Model AVO-9A-B
40 mA/DIV
1 ns/DIV

Each of the 19 models in the Avtech AVO-9 series of pulsed laser diode drivers includes a replaceable output module with an ultra-high-speed socket suitable for use with sub-nanosecond rise time pulses. Models with maximum currents of 0.1A to 10A are available with pulse widths from 400 ps to 1 us. GPIB, RS-232, and Ethernet control available.

AVTECH
Nanosecond Electronics
Since 1975

Pricing, manuals, datasheets and test results at:
http://www.avtechpulse.com/laser

2 to 200 Amp Current Pulsers

Avtech has pioneered the design of user-friendly 2 to 200 Amp constant current pulsers. We offer over 35 models in five series for laser diode, air bag, squib, fuse and other applications. The basic specifications are as follows:

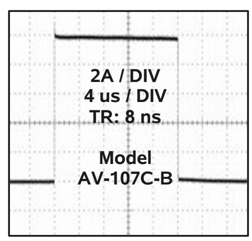

Series	I, V	PW	TR
AV-107	2 - 20 A, 60 V	0.2 - 200 us	10 - 30 ns
AV-106	5 - 100 A, 100 V	0.5 us - 1 ms	50 ns - 1 us
AV-108	12.5 - 200 A, 100V	2 us - 1 ms	5 - 15 us
AV-109	10 - 100 A, 5 V	10 us - 1 s	10 us
AV-156	2 - 30 A, 30 V	1 us -100 ms	0.2 - 50 us

Avtech has a long history of producing one-of-a-kind custom units.

AVTECH
Nanosecond Electronics
Since 1975

Pricing, manuals, datasheets and test results at:
http://www.avtechpulse.com/current

The Right RF Parts. Right Away.

We're RF On Demand, with over one million RF and microwave components in stock and ready to ship. You can count on us to stock the RF parts you need and reliably ship them when you need them. Add Fairview Microwave to your team and consider it done.

Fairviewmicrowave.com
1.800.715.4396

Fairview Microwave
an INFINITe brand

SAM KUSANO | Industry Expert, Communication Solution Group, Keysight Technologies Inc.
www.keysight.com

Modulation Distortion:

An Innovative Method for High-Accuracy EVM Measurements

Error vector magnitude is a critical parameter for power amplifiers. Here's an approach that combines a VNA and VSG with a modulation-distortion application to overcome measurement challenges.

In wireless communication systems, power amplifiers (PAs) make a significant contribution to the quality attained in the RF chain. These components play a critical role in determining the condition of the communication service in terms of signal quality and battery life.

PAs are positioned in the last stage of the transmission chain and generate the RF power that's then transmitted over the antennas. PA designers aim to maximize linearity while maintaining a high level of efficiency. This balance is challenging to achieve across extremely wide signal bandwidths in the millimeter-wave (mmWave) frequency spectrum.

To measure the nonlinearity of a PA under a modulated stimulus condition, the industry uses error vector magnitude (EVM) as a figure of merit (FOM) for in-band characteristics and adjacent channel power ratio (ACPR) for out-of-band characteristics. This article introduces an innovative method called modulation distortion (MOD) for characterizing the nonlinearity of a PA under modulated stimulus conditions.

To measure the nonlinearity of a PA under a modulated stimulus condition, the industry uses error vector magnitude (EVM) as a figure of merit (FOM) for in-band characteristics and adjacent channel power ratio (ACPR) for out-of-band characteristics.

CHALLENGES IN DEVICE CHARACTERIZATION UNDER WIDEBAND MODULATED SIGNALS

The introduction of 5G new radio (NR) means that designers need to perform EVM measurements using extremely wide signal bandwidths in the mmWave spectrum. A vector signal generator (VSG) combined with a vector signal analyzer (VSA) are traditionally used to measure EVM. However, it's challenging to measure EVM with these test instruments due to several reasons:

Errors contributed by the stimulus

In the VSA method, the error vector is the value obtained when comparing the ideal signal with the measured signal for each constellation. The integrity of the signal source has a direct impact on the measurement result. The distortion of the generated signal needs to be lower than the distortion generated by the device under test (DUT).

The VSA method is also sensitive to I/Q imbalance and phase noise not normally created by the DUT. In addition, the signal-to-noise ratio (SNR) decreases as the bandwidth (BW) of the signal gets wider and generates noise. Random noise at low power levels can result in less accurate and reliable EVM measurements.

Errors contributed by the receiver

To minimize any errors in the EVM measurement result, the input signal needs to be digitized using a signal analyzer that does not produce any nonlinear distortion. Furthermore, the noise floor of the receiver must be lower than the target signal. This is especially challenging to accomplish across wider signal BWs since the SNR of the receiver is also lower.

To manage the input level of the receiver chain, the attenuation and gain settings of a receiver chain need to be carefully controlled, which requires deep knowledge of the analyzer. Iterating across different input levels and settings to optimize receiver optimization slows down the measurement process.

Signal fidelity

In the VSA method, there are multiple ways to calibrate the test system. The most advanced technique compensates for the I/Q waveform so that the input signal is a flat response at the reference plane. This method may include an error, especially when the test signal has a wide BW and the DUT has poor mismatch.

MOD ON A PNA-X VNA

Modulation distortion offers a new approach to overcome the measurement challenges associated with the VSA method. By combining the following PNA-X, VSG, and MOD application, users can characterize the nonlinear distortion of a device under a modulated signal and establish FOMs, including EVM and ACPR *(Fig. 1)*.

Since the entire measurement setup is integrated into the PNA-X firmware, the user can easily configure the stimulus and establish the measurements. Also, the measurement leverages state-of-the-art calibration techniques for optimum accuracy.

On top of that, the MOD application enables users to access additional measurements besides the typical PNA-X measurements, such as S-parameters, gain compression, intermodulation distortion (IMD), and noise figure. The MOD application on the PNA-X also supports nonlinear distortion measurements under a modulated stimulus condition without the need to change the connection.

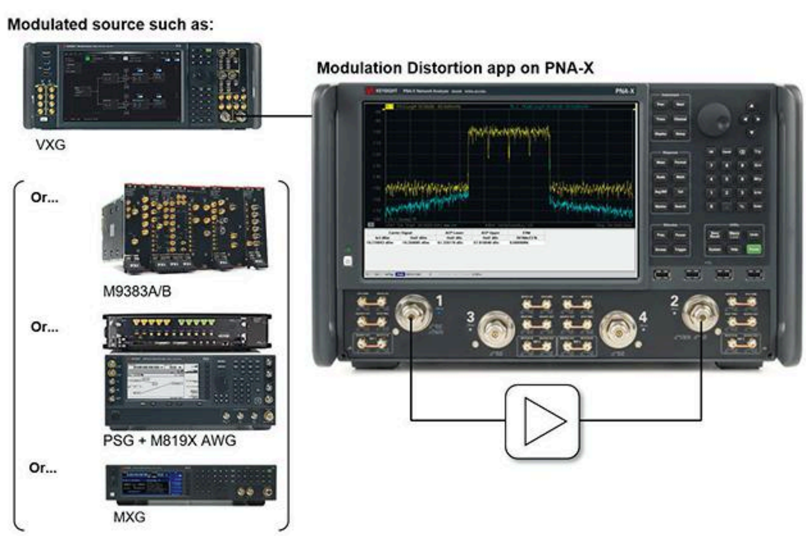

1. MOD is a software application that runs on the PNA-X. It provides an innovative approach for performing device characterization under wideband modulated signals.

Low Noise BYPASS AMPLIFIERS

1 MHz to 43.5 GHz

- *Built-in bypass and shutdown*
- *Noise figure as low as 1.1 dB*
- *Ultra-wide bandwidths with flat gain*

Mini-Circuits®

www.minicircuits.com P.O. Box 350166, Brooklyn, NY 11235-0003 (718) 934-4500 sales@minicircuits.com 584 Rev A_P

After the MOD application measures the vector-corrected input and output spectrum with a corrected receiver and the desired modulated waveform, the MOD application processes the data by comparing the input spectrum and output spectrum. The technique is called spectral correlation.

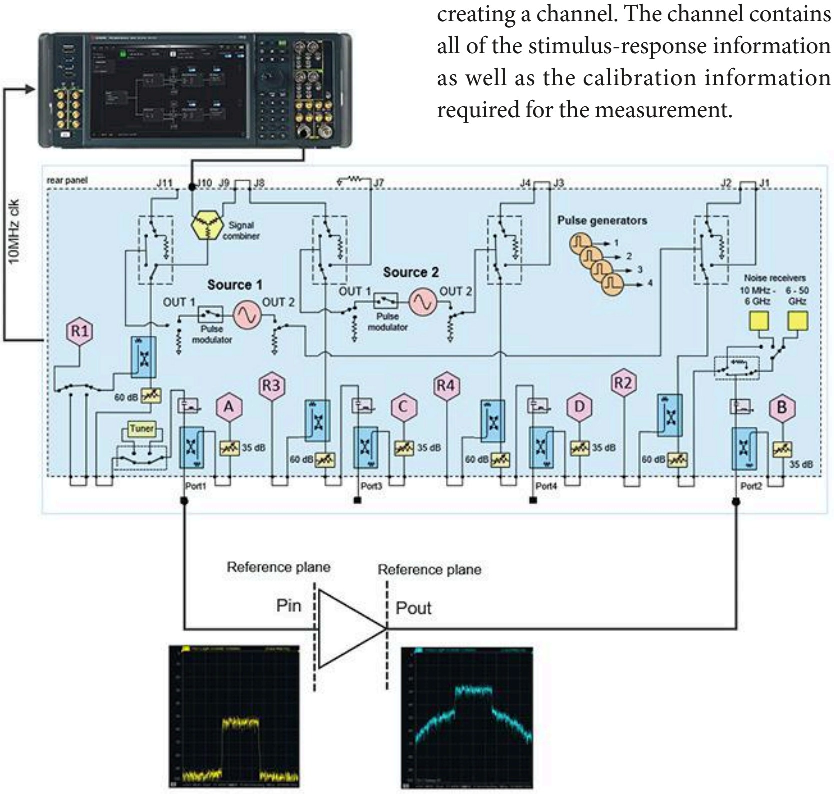

2. This is a block diagram of the measurement system consisting of a PNA-X and a VSG.

PNA-X UNIQUE IMPLEMENTATION

Figure 2 shows the block diagram of the measurement system consisting of a PNA-X and a VSG:

- The output of the VSG is connected to the rear panel of the PNA-X (J10) so that the signal can go through the internal path of the PNA-X.
- The modulated signal is then made available from test port 1 (connected to the DUT) of the PNA-X.
- Test port 2 of the PNA-X is connected to the output of the DUT.
- Input and output spectrum of the modulated signal use receivers R1, A, and B, coherently.

All of the required configurations to make a measurement can be completed with the MOD software application integrated into the firmware of the PNA-X. Similar to other application software that runs on a PNA-X, measurements start by creating a channel. The channel contains all of the stimulus-response information as well as the calibration information required for the measurement.

The calibration of the measurement system plays a critical role when making an accurate measurement. The MOD method offers two different types of calibrations to accurately perform EVM and ACPR measurements:

- A linear calibration plane is first established to remove the linear error from the raw measurement result. This can be achieved by the same process as the other measurement class of PNA-X.
- The modulated source correction is then performed to generate the desired modulated waveform at the reference plane.

After the MOD application measures the vector-corrected input and output spectrum with a corrected receiver and the desired modulated waveform, the MOD application processes the data by comparing the input spectrum and output spectrum. The technique is called spectral correlation. With this advanced data processing approach, the MOD decomposes the spectrum into a linearly correlated part and a distortion part. Subsequently, the MOD application computes the FOM such as EVM and ACPR. The correlation of the FOM to the traditional VSA method is mathematically proven, along with actual measurements of the PA.

NEW METHOD FOR CHARACTERIZING PA NONLINEAR DISTORTION

Device characterization under wideband modulated signals is a significant challenge. 5G requires PA designers to perform EVM measurements using extremely wide signal bandwidth in the mmWave spectrum. The traditional method using a VSA and VSG is no longer enough. Design engineers need a new method to measure critical parameters for PAs such as EVM and ACPR. The PNA-X MOD application provides various benefits to PA characterization, including:

- *MOD overcomes wideband measurement challenges.* The wide dynamic range of the PNA-X enables low residual EVM due to wider system dynamic range (lower noise floor). Also, easy calibration for "vector-corrected" measurements enables signal fidelity at the DUT input. As a result, measurement reproducibility improves significantly.
- *Design flow improvement with simulation.* The same computation engine as the PNA-X to simulate nonlinear behavior is available in the Keysight ADS simulation environment. This enables PA designers to accelerate the design cycle.
- *MOD leverages PNA-X hardware to perform analysis under modulated conditions.* For any PA characterization, a VNA is essential to characterize linear and nonlinear performance. By adding the MOD application with a modulated source, the test system makes traditional VNA measurements as well as ACPR and EVM. Also, the unique architecture of the PNA-X allows users to perform multiple measurements with a single connection (touch down). mw

SAM KUSANO is an industry expert for Keysight Technologies' communication solution group. He has over 19 years of experience in measurement applications for RF test equipment, such as the vector network analyzer, signal generator, and signal analyzer. Sam started his career in research and development at Agilent Technologies in 2001, designing RF and microwave circuits. Since 2007, he has been a marketing engineer, application engineer, and industry expert in the wireless communication industry. Sam received a Master's in applied physics at Kyushu University, Japan in 2001.

5G requires PA designers to perform EVM measurements using extremely wide signal bandwidth in the mmWave spectrum. The traditional method using a VSA and VSG is no longer enough. Design engineers need a new method to measure critical parameters for PAs such as EVM and ACPR.

JUSTIN POLLOCK | Senior Antenna Engineer, KP Performance Antennas
www.kpperformance.com

SCADA: Alive and Well in the Age of IoT

Despite the onslaught of the Internet of Things within the industrial world, SCADA will continue to evolve to meet today's demands.

When most people think of the Internet of Things (IoT), home automation is what comes to mind. But in terms of complexity, home automation is a simple network compared with applications in "smart" cities, huge manufacturing facilities, and eventually connecting everything necessary to enable vehicle autonomy.

However, IoT may have some of its greatest impact on the utilities market and others considered mission-critical. They have been using supervisory control and data acquisition (SCADA) systems for decades to monitor and control far-flung assets of industrial, government, energy, and other industries. IoT and SCADA are different in many ways, but the former is so all-encompassing it's certain to influence SCADA. The question now is how.

For those not familiar with SCADA, it's a supervisory system designed to monitor and control critical equipment usually dispersed over a large area. It's a crucial technology for ensuring reliable operation of systems ranging from water and waste control to energy distribution, oil and gas refining, transportation, fossil-fuel and nuclear power plants, and many others. Without SCADA, these systems would function "in the dark" with no feedback concerning the status of their hundreds to tens of thousands of sensitive areas.

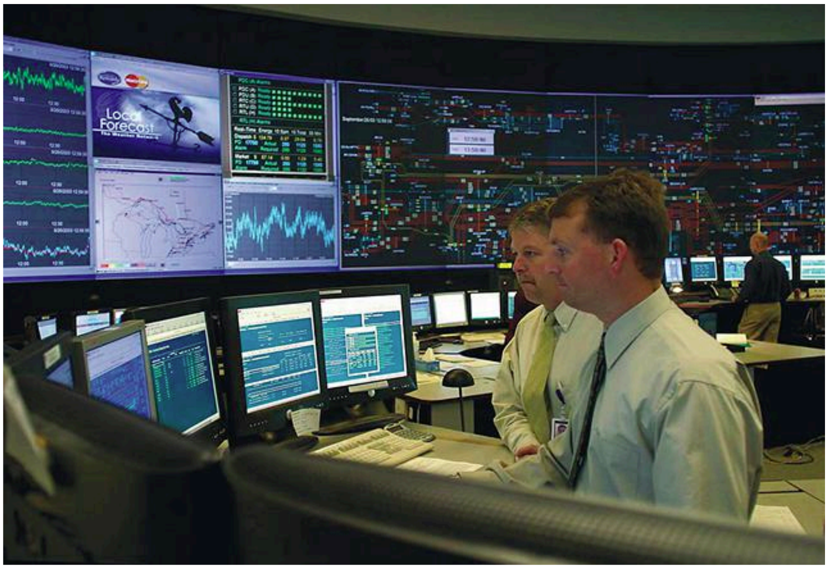

1. The control center of a large organization gets its raw data from sensors in the SCADA system. *(Source: All About Circuits)*

SCADA systems offer two basic functions: remote control of equipment such as power switches and breakers, including load control/load shedding, valves and actuators, and telemetry to report their current status to a central point. They also allow for remote measurement and reporting of more detailed data sensors connected to these and other devices.

The concept was conceived at least as far back as the 1930s to provide supervisory control of electric utilities and has been updated periodically over the years to increase performance and reduce human intervention. A system consists of hardware, software, wired and wireless communications, and programmable logic controllers (PLCs) and remote terminal units (RTUs) to which are connected various types of sensors. Atop all of this hardware sits SCADA's supervisory capabilities.

The data from the sensors or RTUs can be transmitted via any means available, from telephone lines to Ethernet, satellite, or wireless sensor networks (WSNs), depending on what's available and cost-effective. A variety of wired protocols continue to be used, some dating back to the earliest SCADA deployments, although the trend is toward open-source protocols to eliminate dependence on proprietary solutions.

The information from the sensors is sent to a control center where all points in the system are displayed. In a large industrial facility or utility network control center *(Fig. 1)* is a wall of monitors with a striking resemblance to NASA Mission Control. A SCADA system also has a "historian" feature, a database of time-stamped data about alarms, measurements, and other types of information that can be used for statistical analysis.

SCADA AND IIoT

With the emergence of the industrial IoT (IIoT), there are differing opinions about what will become of SCADA, ranging from SCADA complementing IoT, to SCADA gradually disappearing within IIoT. However, the smart money is on SCADA not just surviving, but expanding its supervisory role by adding some of the features employed by IoT. This includes edge- and cloud-based processing and analytics that enable automated preventative and ultimately prescriptive maintenance, thus lessening reliance on human intervention.

SCADA won't disappear any time soon for the simple reason that deployed SCADA systems dwarf IIoT deployments today. And this will be the case for years, because they are an essential ingredient in mission-critical systems that have been deployed and modified multiple times over decades. These systems include nuclear reactors, defense operations, the power grid, the entire fossil-fuel industry, and many more. Wholesale replacement of these systems with pure IIoT solutions would also be prohibitively expensive and immensely disruptive, potentially leaving some assets unprotected from cyberattack during the transition.

So, it shouldn't be surprising that SCADA represents a substantial portion of the global market for industrial control systems, which is projected to be nearly $200 billion by 2024. In short, while IIoT will continue to permeate more industry sectors, SCADA will continue to provide its traditional functions of alarming, data logging, real-time control, and database management—only better.

NEW WAVES IN WIRELESS SCADA

Traditionally, wireless SCADA used a self-provided network specifically designed to minimize single points of failure that alone could take an entire system down. To achieve this, many advances have been made to enhance this resilience by providing redundant signal paths, mesh-type network topologies, and various wireless systems and technologies.

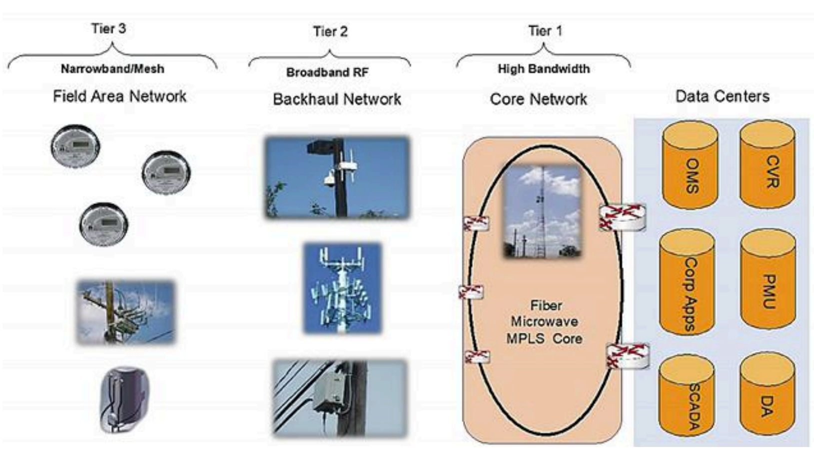

2. The three tiers of a utility telecommunications architecture consist of a field area network, backhaul, and the high-throughput network core. *(Source: Utilities Technology Council; prepared by Red Rose Telecom)*

Utilities and other mission-critical industries long ago decided that the only way to ensure "five nines" reliability was to build their own wired and private wireless networks. It was believed that commercial networks were not reliable enough and because much utility infrastructure is located in places not served by commercial carriers. As a result, utilities today own at least 80% of their own communications networks and use commercial systems sparingly. The networks originally served only voice communications, but when SCADA began its deployment, data was added to the mix and today consists of much of the traffic.

That said, other industries not designated as mission-critical use nearly all common standards and protocols, from unlicensed industrial, scientific and medical (ISM) bands at 902 to 928 MHz, 2.4 GHz and 5.7 GHz, WiMAX, TETRA, second- and third-generation cellular access methods, digital mobile radio (DMR), and private land-mobile radio systems. Satellite-based systems are also in widespread use, especially by industries whose assets are geographically diverse, a good example of which is the distribution of oil and gas and offshore drilling.

Point-to-point and point-to-multipoint RF and microwave links have been a mainstay of SCADA for many years, making it possible to connect widespread assets while also delivering high data rates and high reliability. The power grid illustrates where microwave links and other wireless technologies play a role in a complex, geographically massive network, which can be divided into three tiers *(Fig. 2)*. Tier 1, the network backbone, is served by fiber-optic and point-to-point microwave links in a ring topology so that any site can communicate to the central site via two completely different paths. Most utilities used licensed frequencies around 6 GHz for this purpose.

As always, fiber is the preferred transmission medium, but it's very expensive and often nearly impossible to deploy, especially in remote areas. As a result, microwave links account for at least half the backbone infrastructure. They can deliver very-high-speed connectivity over many hops throughout a wide geographical area. Up to four radios are typically installed on a tower. The protocol in both cases is typically Carrier Ethernet, although others are used as well.

The benefit of microwave links is their ability to send information over long distances with a minimum amount of infrastructure, using cost-effective tower-mounted antennas. For example, the KP-5PDN-2 *(Fig. 3)* is a versatile 2-ft. parabolic antenna with N-type connectors covering 4.9 to 6.4 GHz with gain of 30 dBi. Its highly directional pattern reduces interference and provides a reliable link over paths of tens of miles. The YA17KPPD is a rugged, industrial yagi antenna operating between 880 and 948 MHz with 17 dBi of gain and can withstand heavy ice, high wind, and other harsh environmental conditions.

The second tier is connected using point-to-point microwave links for provision of telemetry and backhaul to substations that are connected to the Tier 1 backbone. One of the main problems currently faced by utilities is lack of available spectrum nearly anywhere at 6 GHz and below, so they must cope with sharing frequencies using the FCC's new Citizens Broadband Radio Service (CBRS) at 3.5 GHz.

Frequency sharing is becoming more common today, owing to the lack of available spectrum. However, for mission-critical applications, it leaves a lot to be desired. That is, the allocated spectrum is divided into three classes, the first being incumbents (primarily government radars). These incumbents must be protected from interference from licensed Priority Access Licensees (PAL). The lowest class, unlicensed General Authorized Access (GAA) users, has no protection from the upper classes and must not interfere with them. As CBRS is just now being deployed, it remains to be seen how well this extremely complex system will work as another frequency-sharing scenario, because the so-called white-space frequencies between 470 and 790 MHz have suffered significant issues.

3. The KP-5PDN-2 2-ft. parabolic antenna covering 4.9 to 6.4 GHz has gain ranging from 27.5 to 29.8 dBi, depending on frequency. This increases the input power from a maximum of 50 W to an EIRP nearly 10 times that, enabling long distances to be covered.

The third tier is the one that resembles what most people would consider IoT as it consists of many sensors and RTUs served by a low-power, low-speed network using narrow channels at 900 MHz. Tier 3 is typically a much more localized solution. Nevertheless, it increasingly requires higher data rates to carry high-resolution video that's in limited use today, but will likely be a required capability in the future.

As 6 GHz is one of the primary frequencies used by utilities for SCADA, emergency management, and land-mobile radio, there's increasing concern about an FCC Notice of Proposed Rulemaking that would allow use of the 5.925- to 7.125-GHz band for unlicensed operation by other services. Like every snippet of potentially available spectrum, this one is contentious because of the potential for interference to other services operating on or near each other.

However, for mission-critical infrastructure, sharing of spectrum presents potential national security issues, which is why it has always relied on its own networks operating licensed frequencies. Nuclear power plants, for example, rely almost entirely on 6-GHz systems for backhaul communications. Utilities were already spectrally "refarmed" once from frequencies around 2 GHz in the 1990s, at massive cost, to make way for commercial services.

If this happens again, the alternatives are at 8 and 11 GHz, whose propagation characteristics are less favorable than 6 GHz for spanning distances between microwave radios. Consequently, this would require more than simply changing frequencies in hardware. Coverage analysis would be needed on a huge scale, along with moving existing towers and adding new ones, including their installed equipment like parabolic antennas. As of this writing, no decision has been made about how this spectrum will be used.

IIoT AND SCADA

The emergence of IoT has already created one possible opportunity for organizations that use SCADA: Competition between the cellular industry and LPWAN providers for providing connectivity between IoT deployments and the internet. Both offer solutions designed specifically for connecting vast numbers of devices that transmit minimal amounts of data.

Cellular carriers offer the LTE-M and narrowband IoT (NB-IoT) protocols for this purpose, while LPWANs are increasingly centered on two solutions, Sigfox, and variations of the LoRa protocol, such as LinkLabs Symphony Link. The difference between these solutions and 4G is their focus on the needs of small, typically battery-operated devices rather than delivering blazingly fast speeds required for consumer applications.

2 GHz Clock Generator

- *Square wave clocks from DC to 2.05 GHz*
- *Random jitter <1 ps (rms)*
- *80 ps rise and fall times*
- *16-digit frequency resolution*
- *CMOS, LVDS, ECL, PECL, RS-485*
- *Phase adjustment & time modulation*

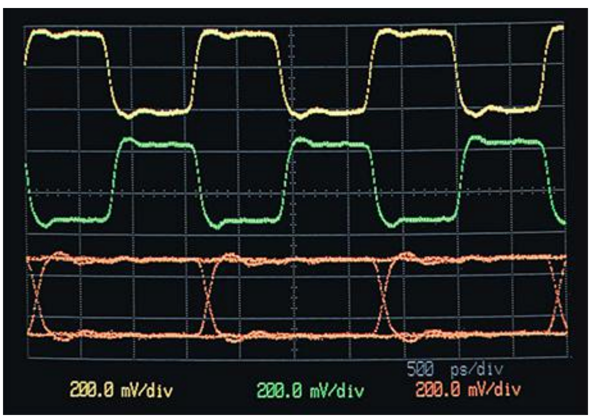

Plot shows complementary clocks and PRBS (opt. 01) outputs at 622.08 Mb/s with LVDS levels. Traces have transition times of 80 ps and jitter less than 1 ps (rms).

The CG635 generates clock signals—flawlessly. The clock signals are fast, clean and accurate, and can be set to standard logic levels.

How fast? Frequency to 2.05 GHz with rise and fall times as short as 80 ps.

How clean? Jitter is less than 1 ps and phase noise is better than –90 dBc/Hz (100 Hz offset) at 622.08 MHz.

How accurate? Using the optional rubidium timebase, aging is better than 0.0005 ppm/yr, and temperature stability is better than 0.0001 ppm.

You would expect an instrument this good to be expensive, but it isn't. You no longer have to buy an rf synthesizer to generate clock signals. The CG635 does the job better—at a fraction of the cost.

SRS

Stanford Research Systems

Phone: (408)744-9040 • info@thinkSRS.com • **www.thinkSRS.com**

Operators of mission-critical infrastructure would argue that while cellular wireless networks are the undisputed leaders in providing ubiquitous coverage, they're still commercial systems, and do not meet their demanding requirements for reliability. In addition, carriers and LPWAN providers charge a fee for every node they connect. In the case of LPWAN specifically, coverage is a tiny fraction of what cellular offers, and as a competitor to the cellular behemoth, is not certain to survive.

That said, in order to adequately serve "Industry 4.0," both services must find a way to connect devices with either minimal or no modern connections—wired or wireless. These could be pumps that have been in service for years but still work fine, are expensive, and would be senseless to replace if only for becoming part of a modern network.

The solution to this issue is "bolting-on" connectivity. This can be done via an inexpensive device that senses changes in some critical operating characteristic (like noise or vibration), converts the analog sensor to digital form, and communicates it to a gateway via one of the various short-range wireless protocols used for IoT (Zigbee, Bluetooth, Z-Wave, etc.).

However, issues arise when employing this approach in the SCADA environment, whose sensors typically use wired connections to the RTU or, like some of their legacy industrial counterparts, have no connectivity at all. Many of the locations monitored by SCADA are far from civilization and experience environmental conditions far more hostile than comparatively benign industrial settings. This is not an insurmountable problem in most cases, as some form of protection can be added to encase the device, assuming the addition is actually worth the effort.

Another fundamental issue when considering IoT integration with SCADA is whether it's worth the risk, since access to the internet is IoT's mandatory requirement. In SCADA, nearly all decision-making, limited though it may be when compared with IoT, resides at the PLC or RTU, which eliminates the ever-more onerous issues with internet security. With IoT, decisions are made locally as well, increasingly in edge computers and gateways, but the data eventually finds its way to a cloud data center—via the Internet.

SUMMARY

IoT may be taking the industrial world by storm, but it won't replace SCADA systems, at least not in the foreseeable future. Instead, SCADA will take those IoT elements that benefit it, such as advanced sensors, and eventually have the ability to perform preventative and prescriptive maintenance. Right now, SCADA's biggest challenge is arguably finding frequencies in which it can perform its mission-critical functions without interference from other services. Once this problem is solved, it has a clear path toward advancing from a supervisory to a fully automated solution, employing high-resolution artificial intelligence and many other technologies. mw

MILLIMETER WAVE MMIC PRODUCTS

MULTI-OCTAVE BANDWIDTHS
UP TO 43.5 GHz

Attenuators | Couplers | Mixers
Multipliers | Reflectionless Filters | Splitter/Combiners

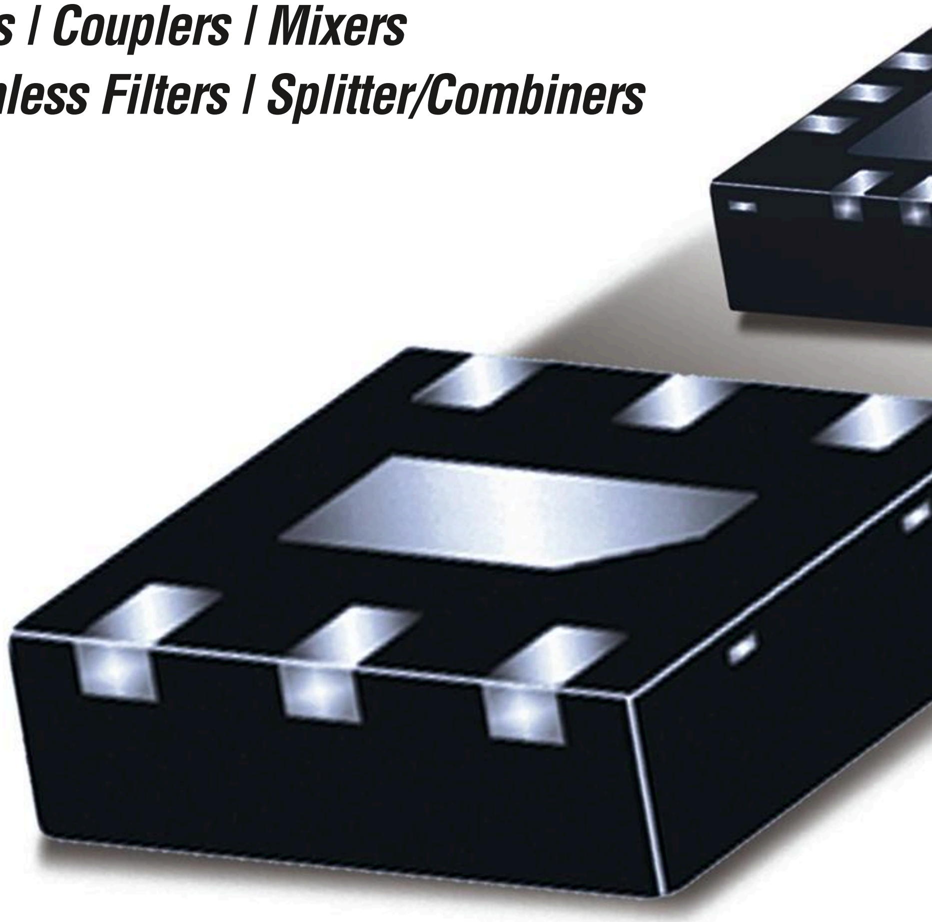

Now over 60 MMIC models *In Stock*
covering applications above 26 GHz

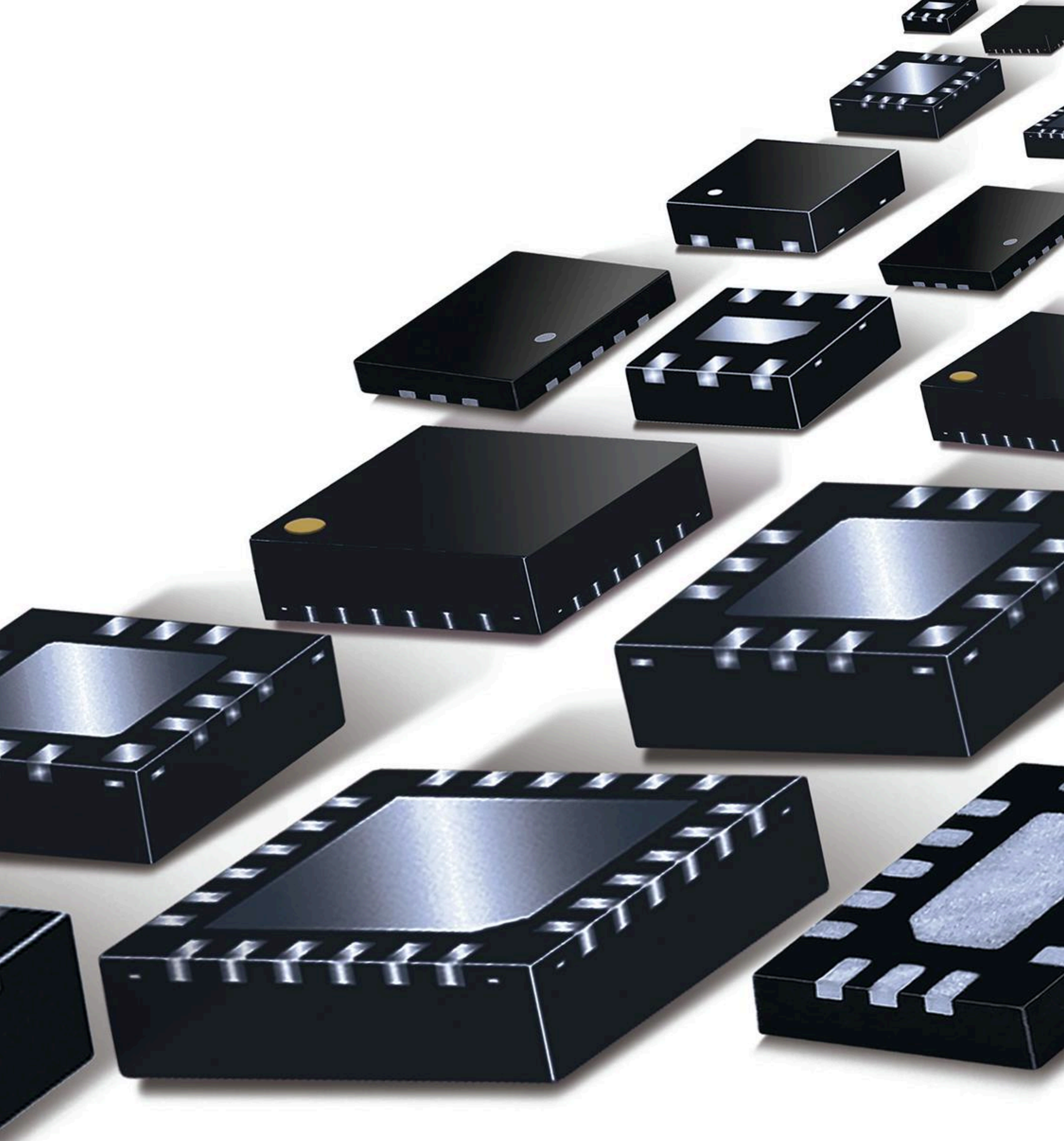

Available in Plastic SMT & Unpackaged Die

Design Feature

SIAMACK GHADIMI | Research and Development, Infineon
www.infineon.com

Determining Volterra Kernels for Nonlinear RF Power Amplifiers

Various methods are used to estimate Volterra kernels, but two other different approaches can make that job easier. RF PA experiments chronicled here help support that claim.

The two methods presented in this article estimate first-, third-, and fifth-order Volterra kernels for an RF power amplifier (PA) using common RF laboratory instruments. In the first method, single measurement readings are employed to determine the kernels, while the second approach utilizes least-squares curve adaptation of measured data. Comparisons between the two methods discussed here and others described in existing publications reveal that these methods are easier to perform.

When an amplifier operates in the nonlinear region, it produces unwanted signals, namely harmonics. The second-, third-, and higher-order harmonics are outside of the amplifier's bandwidth and can thus be filtered out. However, unwanted signals close to the fundamental (intermodulation products) cannot be filtered out and will interfere with amplified input signals and cause nonlinearity *(Fig. 1)*. Furthermore, channel selectivity, detection efficiency, quality, and more importantly, spectral efficiency are impacted, leading to poor wireless-network capacity.[1, 2]

To reduce the impact of nonlinear effects, a mathematical model is needed to describe and represent these unwanted signals.[3] Overcoming these signals can be accomplished through various methods, such as feedback reduction.[2]

The Volterra series is a polynomial representation of nonlinear systems.[4] Similar to the Taylor series, the Volterra series serves as a model for nonlinear behavior. In terms of problem solving, the most difficult and crucial aspect involves determining the coefficients of the power series. If the kernels of an amplifier are determined, the Volterra series can be applied for theoretical analysis and simulation of the amplifier.

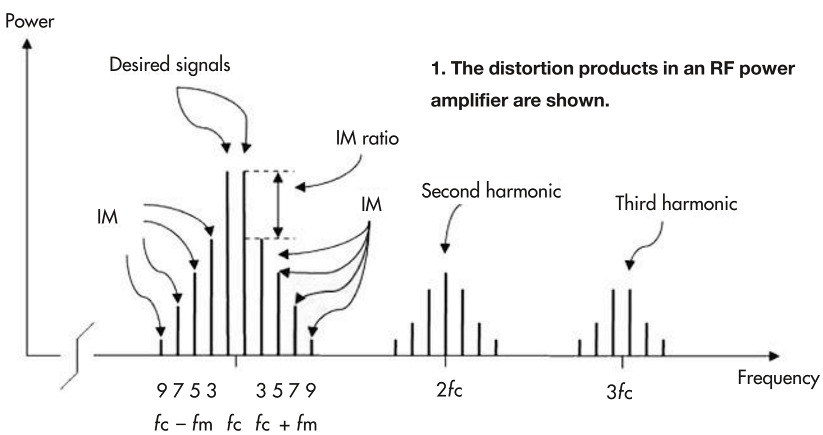

1. The distortion products in an RF power amplifier are shown.

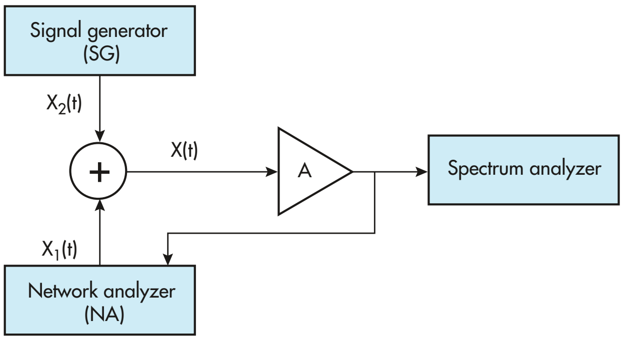

2. This is a principal sketch of the measurement setup.

The complexity associated with determining the Volterra series' coefficients led to the lack of interest in this method. Although the Volterra series is a very good representation of broadband systems, few publications exist on this subject.[5, 6, 7]

There are different types of unwanted signals, such as harmonic and intermodulation (IM) products *(Fig. 1)*. The second-, third-, and higher-order harmonic signals can simply be filtered out because they are far away in frequency from the desired signals. However, the IM signals (third-, fifth-, seventh-, and ninth-orders) are located near the desired signals, making it impossible to filter them out. As mentioned, this will lead to a lower system spectral efficiency.[6]

The main focus of this work is the broadband RF PA, which experiences frequency-dependent nonlinearity. Frequency-independent nonlinearity occurs in a narrowband RF PA.

Nonlinear systems, such as RF amplifiers, have two kinds of nonlinearities: the nonlinearity between the amplitudes of the input and output signals and the nonlinearity between the phases of the input and output signals. These two nonlinearities are divided into two categories: memory-less systems and systems with memory.[2]

The nonlinearity of the memory-less systems is frequency-independent. In other words, these systems do not have any inductors or capacitors. If we ignore the phase, the mathematical representation of these systems is:[4]

$$y(t) = k_1 x(t) + k_2 x^2(t) + k_3 x^3(t) + \ldots \tag{1}$$

If we do not ignore the phase, the nonlinearity is represented by a complex power series:

$$y(t) = k_1 e^{j\phi_1} x(t) + k_2 e^{j\phi_2} x^2(t) + k_3 e^{j\phi_3} x^3(t) + \ldots \tag{2}$$

where $k_1{}^{ej\varphi 1}$, $k_2{}^{ej\varphi 2}$,… are constants.

In systems with memory, the nonlinearity is frequency-dependent—for example, an RF amplifier. In these systems, nonlinearity is described by the Volterra kernel, which is also called a power series with memory.[2, 4, 6]

$$y(t) = H_1(f)x(t) + H_2(f)x^2(t) + H_3(f)x^3(t) + \ldots \tag{3}$$

Suppose we have a system with two input signals of different frequencies (we will call them f_1 and f_2). By using the Volterra series equation, all of the terms that have $H_2(f)$, $H_4(f)$, $H_6(f)$… are dropped because they are far away from the desired frequency. These terms are simply filtered out, and we have:

$$y(t) = H_1(f)x(t) + H_3(f)x^3(t) + H_5(f)x^5(t) + \ldots \tag{4}$$

This experiment tries to estimate the Volterra kernels $H_1(f)$, $H_3(f)$, and $H_5(f)$ in a frequency band for an RF amplifier. The reason for not tracing higher-order kernels is that, practically speaking, it's very hard to specify them.

Because the amplifier is band-limited and our interest lies in the IM signals around f_1 and f_2, we can ignore all other frequency bands except the frequency band around f_1 and f_2. Note that the band-limited amplifier is not specified for frequencies much larger than f_1 and f_2. Thus, Equation 4 can simplify to:

$$\begin{aligned} y(t) =& H_1(f)A\sin(w_1 t) + H_1(f)A\sin(w_2 t) + \\ & \frac{9}{4}H_3(f)A^3\sin(w_1 t) + \frac{9}{4}H_3(f)A^3\sin(w_2 t) + \\ & \frac{25}{4}H_5(f)A^5\sin(w_1 t) + \frac{25}{4}H_5(f)A^5\sin(w_2 t) + \\ & \frac{3}{4}H_3(f)A^3\sin((-w_2 + 2w_1)t) - \\ & \frac{3}{4}H_3(f)A^3\sin((w_1 - 2w_2)t) + \\ & \frac{25}{8}H_5(f)A^5\sin((-w_2 + 2w_1)t) - \\ & \frac{25}{8}H_5(f)A^5\sin((w_1 - 2w_2)t) + \\ & \frac{5}{8}H_5(f)A^5\sin((3w_1 - 2w_2)t) - \\ & \frac{5}{8}H_5(f)A^5\sin((2w_1 - 3w_2)t) \end{aligned} \tag{5}$$

We can represent Equation 5 as follows:

$$y(t) = y_{f_1} + y_{f_2} + y_{f_3} + y_{f_4} + y_{f_5} + y_{f_6} \tag{6}$$

where $f_3 = 2f_1 - f_2, f_4 = 2f_2 - f_1, f_5 = 3f_1 - 2f_2, f_6 = 3f_2 - 2f_1$

Nonlinear systems, such as RF amplifiers, have two kinds of nonlinearities: the nonlinearity between the amplitudes of the input and output signals and the nonlinearity between the phases of the input and output signals. These two nonlinearities are divided into two categories: memory-less systems and systems with memory.[2]

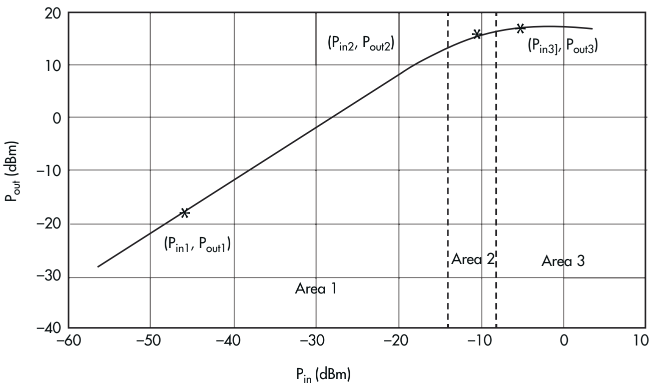

3. Plotted is the output power as a function of the input power at f_1. In Area 1, the first-degree nonlinearity dominates. In Area 2, the first- and third-degree nonlinearities dominate. Lastly, the first-, third-, and fifth-degree nonlinearities dominate in Area 3.

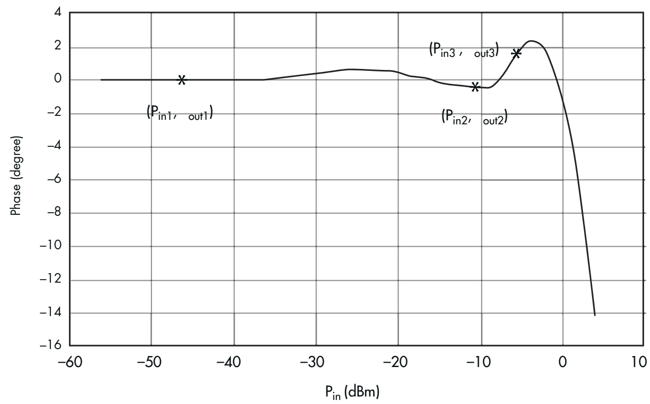

4. Shown is the angle of the frequency f_1 as a function of the input power.

and:

$$y_{f_1} = H_1(f) A \sin(w_1 t) + \frac{9}{4} H_3(f) A^3 \sin(w_1 t) + \frac{25}{4} H_5(f) A^5 \sin(w_1 t) \quad (7)$$

where yf_1 is part of $y(t)$, which contains only the frequency f_1. The expressions containing other frequencies can be obtained in a similar manner.

The Volterra kernels are complex numbers and can be represented in rectangular or exponential form. In this experiment, the exponential form has been chosen, which means six terms should be estimated: H_1, φ_1, H_3, φ_3, H_5, and φ_5.

$$H(f) = |H(f)| e^{j\angle H(f)} = He^{j\phi} \quad (8)$$

METHODS FOR DETERMINING THE VOLTERRA KERNELS

Figure 2 shows the principle sketch of the circuit diagram used to perform measurements. The amplifier's input signal is created by adding a signal from the network analyzer (NA), $x_1(t)$, and a signal from the signal generator (SG), $x_2(t)$.

Hence:

$$x(t) = x_1(t) + x_2(t) = A\sin(w_1 t) + A\sin(w_2 t) \quad (9)$$

which yields:

$$P_{in} = \frac{\left(\frac{A}{\sqrt{2}}\right)^2}{Z_{in}} + \frac{\left(\frac{A}{\sqrt{2}}\right)^2}{Z_{in}} = \frac{A^2}{Z_{in}} \quad (10)$$

The input amplitude is:

$$A = \sqrt{Z_{in} P_{in}} \quad (11)$$

METHOD 1

The purpose of this method is to determine points (P_{in}, P_{out}) on the input power curve as well as points (P_{in}, φ_{out}) on the phase curve for the frequency, f_1. We can then apply these points to estimate kernels. The number of points is determined by the number of kernels that need to be estimated. First, look up a point that can be used to estimate $H_1(f)$. Then, look up another point that together with the estimated $H_1(f)$ can be applied to estimate $H_3(f)$, and so on.

First, for the point *(P_{in1}, P_{out1})* in the graph of *Figure 3* in which the amplifier is linear, we estimate $H_1(f)$.

$$y_{f_1}(t) = y_{1f_1}(t) = H_1(f)A\sin(w_1 t) \tag{12}$$

We determine φ_{out1} in *Figure 4* via point P_{in1}. This yields:

$$P_{out_1} = \frac{\left(\frac{|H_1(f)|A}{\sqrt{2}}\right)^2}{Z_{out}} = \frac{H_1^2 A^2}{2Z_{out}} \tag{13}$$

and

$$\phi_{out_1} = \angle(H_1(f)A) = \angle(H_1(f)) = \phi_1 \tag{14}$$

where $A = \sqrt{P_{in1}Z_{in}}$ gives the following equation for H_1:

$$H_1 = \sqrt{\frac{P_{out_1}2Z_{out}}{P_{in_1}Z_{in}}} = \sqrt{\frac{P_{out_1}2}{P_{in_1}}}, \qquad Z_{in} = Z_{out} \tag{15}$$

$$H_1(f) = H_1 e^{j\phi_1} \tag{16}$$

Now, for the second points *(P_{in2}, P_{out2})* and Φ_{out2} in *Figures 3* and *4* in which the first- and third-degree nonlinearity dominate, we estimate $H_2(f)$.

$$\begin{aligned} y_{f_1}(t) =& y_{2f_1}(t) = H_1(f)A\sin(w_1 t) + \\ & \frac{9}{4}H_3(f)A^3\sin(w_1 t) \end{aligned} \tag{17}$$

$$P_{out_2} = \frac{(V_{out_2})^2}{2Z_{out}} = \frac{|y_{2f_1}(t)|^2}{2Z_{out}} = \frac{(y_{2f_1})^2}{2Z_{out}} \tag{18}$$

By using the vector analysis as shown in *Figure 5*, we obtain:

$$\begin{aligned} \phi_1 =& \angle(H_1(f)A) = \angle H_1(f) \\ \phi_3 =& \angle\Big(\frac{9}{4}(H_3(f)A^3\Big) = \angle H_3(f) \end{aligned} \tag{19}$$

Since V_{out2}, φ_{out2}, H_1, φ_1, and A are known, we calculate H_3 and φ_3 with the following equations:

$$H_3 = \frac{4Y}{9A^3} \tag{20}$$

$$\begin{aligned} &\phi_3 = \arctan\Big(\frac{Q}{P}\Big), \qquad Y = \sqrt{P^2 + Q^2} \\ &P = V_{out_2}\cos(\phi_{out_2}) - H_1 A\cos(\phi_1) \\ &Q = V_{out_2}\sin(\phi_{out_2}) - H_1 A\sin(\phi_1) \end{aligned} \tag{21}$$

Finally, H_3 is estimated as:

$$H_3(f) = H_3 e^{j\phi_3} \tag{22}$$

By the same approach, for the third points *(P_{in3}, P_{out3})* and φ_{out3} in the curves in *Figures 3* and *4*, where the first-, third-, and fifth-degree nonlinearity dominate, we estimate $H_5(f)$.

$$\begin{aligned} y_{f_1}(t) =& y_{3f_1}(t) = H_1(f)A\sin(w_1 t) + \\ & \frac{9}{4}H_3(f)A^3\sin(w_1 t) + \frac{25}{4}H_5(f)A^5\sin(w_1 t) \end{aligned} \tag{23}$$

Using the vector analysis in *Figure 6,* we obtain:

$$\begin{aligned} &y_{3f_1} = V_{out_3} = \sqrt{P_{out_3}2Z_{out}} \\ &\angle y_{3f_1}(t) = \phi_{out_3} \end{aligned} \tag{24}$$

$$\begin{aligned} &H_5 = \frac{4T}{25A^5} \\ &\phi_5 = \arctan\frac{L}{K} \end{aligned} \tag{25}$$

where:

$$\begin{aligned} &T = \sqrt{K^2 + L^2} \\ &K = V_{out_3}\cos(\phi_{out_3}) - H_1 A\cos(\phi_1) - \\ &\quad \frac{9}{4}H_3 A\cos(\phi_3) \\ &L = V_{out_3}\sin(\phi_{out_3}) - H_1 A\sin(\phi_1) - \\ &\quad \frac{9}{4}H_3 A\sin(\phi_3) \end{aligned} \tag{26}$$

Finally, the estimated H_5 is:

$$H_5(f) = H_5 e^{j\phi_5} \tag{27}$$

METHOD 2

In this method, the data from frequency f_1 is used. The method is based on the polynomial adaptation. To this end, we shall try to approximate the values $P_{out}(P_{in})$ and $\varphi_{out}(P_{in})$, which is known by the data measurements via the following equation:

$$\begin{aligned} y_{f_1}(A) =& |y_{f_1}(A)|e^{j\angle y_{f_1}(A)} = y_1 A + y_3 A^3 + y_5 A^5 \\ =& H_1(f)A + \frac{9}{4}H_3(f)A^3 + \frac{25}{4}H_5(f)A^5 \end{aligned} \tag{28}$$

where:

$$\begin{aligned} &V_{out} = \sqrt{P_{out}2Z_{out}} \\ &A = \sqrt{Z_{in}P_{in}} \end{aligned} \tag{29}$$

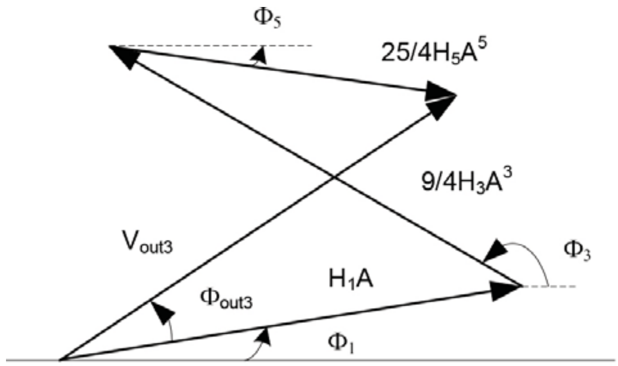

6. Equation 23 is represented by this vector analysis.

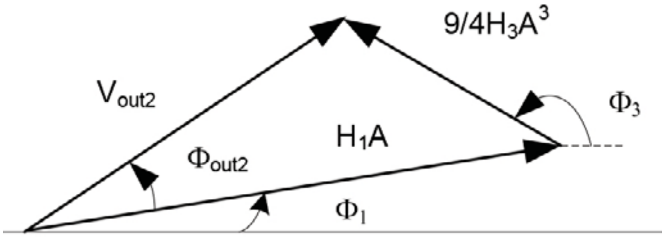

5. This vector analysis describes Equation 17.

and:

$$V_{out}(A) = |V_{out}(A)|e^{j\phi_{out}(A)}$$

(30)

Here, the least-squares method for the polynomial adaptation is used. Hence:

$$\sum_{k=1}^{m}[y_{f_1}(A) - V_{out}(A_k)]^2$$

(31)

This polynomial adaptation yields the values of y_1, y_3, and y_5 in Equation 28. From these values, the kernels, namely $H_1(f)$, $H_3(f)$, and $H_5(f)$, can be easily calculated.[4] To determine the accuracy of this approximation, we can substitute the obtained kernel values in Equation 28 and then vary the input amplitude A and calculate yf_1 for all values of A. This method is easier to implement than the first method and allows for the possibility of estimating higher grades of the Volterra kernels.

In these two methods, the Volterra kernels have been estimated for one frequency, f_1—that is $H_1(f_1)$, $\varphi_1(f_1)$, $H_3(f_1)$, $\varphi_3(f_1)$, $H_5(f_1)$, and $\varphi_5(f_1)$. How-

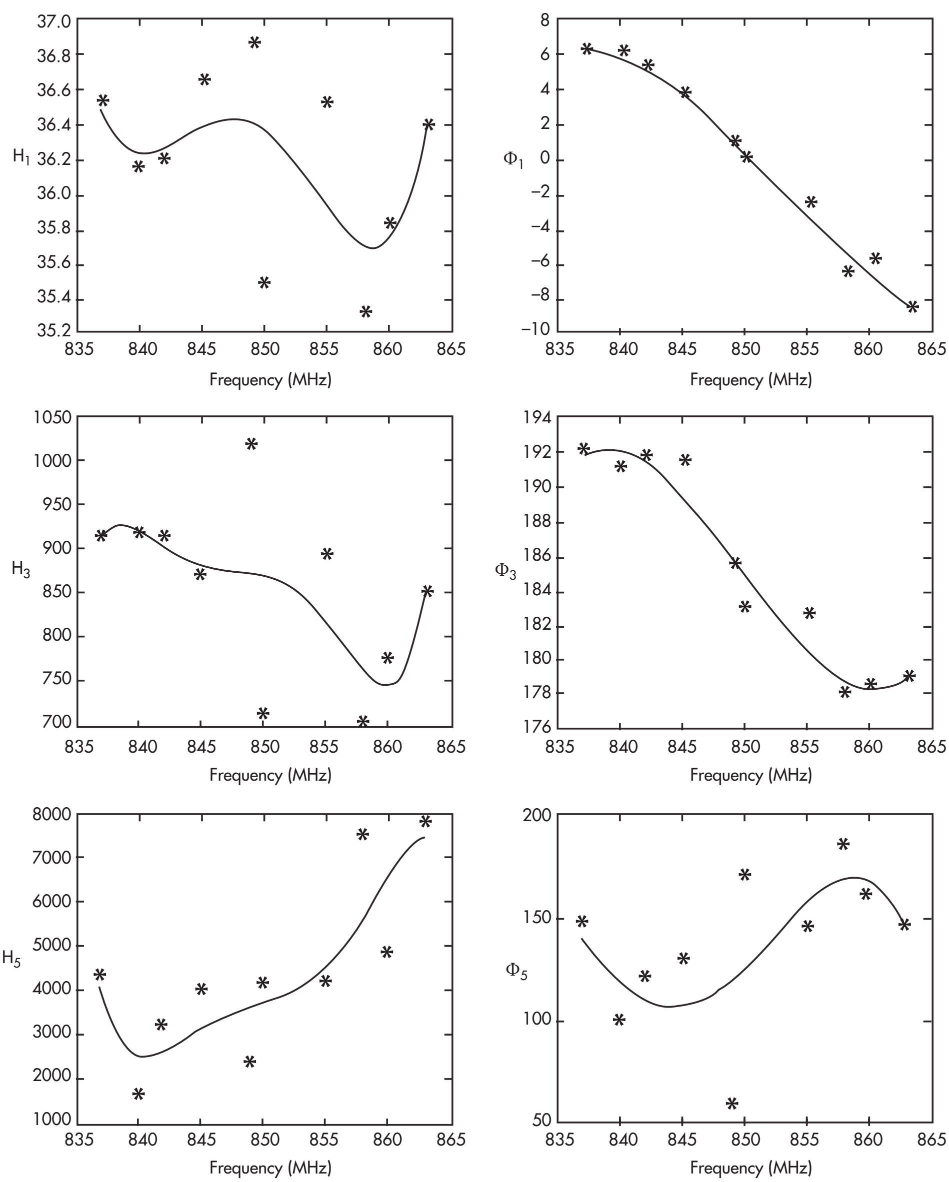

7. Using Method 1, the estimated Volterra kernels are given at different frequencies, as is the frequency dependency of kernels for the bandwidth of 837 to 863 MHz.

ever, it's possible to obtain the kernels for a certain bandwidth by estimating the kernels for some frequencies within the bandwidth. With this approach, we have $H_1(f_{11})$, $H_1(f_{12})$ ... $H_1(f_{1n})$, $\Phi_1(f_{11})$ … $\Phi_1(f_{1n})$, $H_3(f_{11})$ ... $H_3(f_{1n})$ and so on. Finally, by doing a polynomial adaptation with these estimated values, we can obtain the kernels. However, it's required that n be greater than the degree of the adapted polynomial.

MEASUREMENTS AND RESULTS

Measurements are performed on a ZFL-1000H RF PA from Mini-Circuits *(www.minicircuits.com)*. The chosen frequency band is 837 to 863 MHz, which is then divided into 10 narrowband frequency channels (the trial values shown in *Table 1* are from 1.1 to 1.10). Each channel has a 20-kHz bandwidth. Furthermore, measurements are performed for two broadband frequency ranges, with bandwidths of 3 MHz (850 to 853 MHz) and 5 MHz (847 to 852 MHz), respectively.

Trial	H_1	$\phi_1[Deg]$	H_3	$\phi_3[Deg]$	H_5	$\phi_5[Deg]$
1.1	36.5	6.3	911.4	192.0	4299.3	145.9
1.2	36.1	6.1	915.5	191.0	1580.9	98.0
1.3	36.2	5.3	911.6	191.6	3162.8	119.6
1.4	36.6	3.6	868.4	191.4	3960.3	128.6
1.5	36.9	1.0	1014.4	185.3	2331.3	57.5
1.6	35.5	0.0	709.0	182.8	4059.7	170.2
1.7	36.5	-2.6	888.7	182.4	4194.2	144.1
1.8	35.3	-6.5	701.4	177.8	7475.4	184.2
1.9	35.8	-5.7	773.1	178.3	4853.1	159.8
1.10	36.4	-8.6	847.1	178.9	7777.9	145.0

Table 1: Listed are estimated Volterra kernels at different frequencies for f_1 using Method 1.

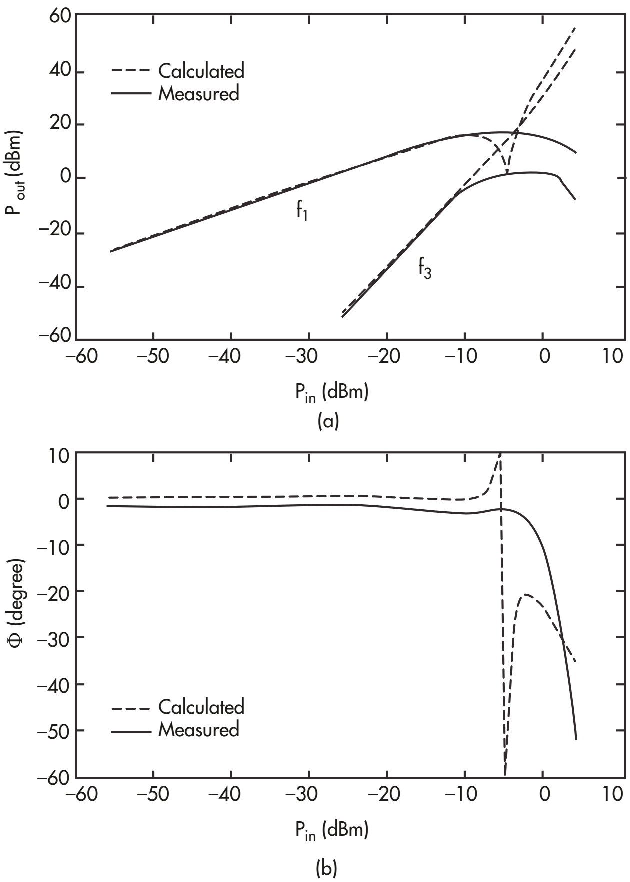

8. In this broadband measurement, f_1 = 850 MHz and f_3 = 847 MHz. Shown are measured and calculated $P_{out}(P_{in})$ curves at frequencies f_1 and f_3 (a), and measured and calculated angles of f_1 (b).

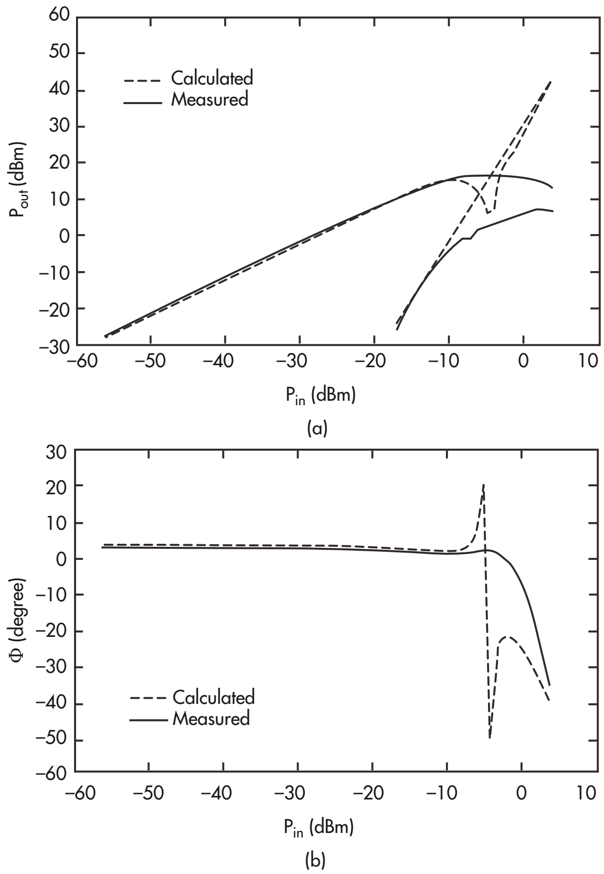

9. In this broadband measurement, f_1 = 847 MHz and f_3 = 842 MHz. Shown are measured and calculated $P_{out}(P_{in})$ curves at frequencies f_1 and f_3 (a), and measured and calculated angles of f_1 (b).

Trial	H_1	$\phi_1[Deg]$	H_3	$\phi_3[Deg]$	H_5	$\phi_5[Deg]$
1.1	34.3	4.8	700.3	181.8	4835.2	1.0
1.2	34.3	4.8	714.0	182.7	4795.9	2.2
1.3	34.8	3.8	747.3	181.5	5200.6	0.9
1.4	35.7	1.9	783.9	179.5	5588.0	-1.1
1.5	34.9	-0.3	756.3	177.0	5281.8	-3.7
1.6	34.4	-0.8	673.9	176.5	4364.9	-4.3
1.7	35.3	-3.9	760.5	173.3	5344.8	-7.3
1.8	34.7	-7.6	728.0	171.7	5127.0	-7.4
1.9	35.1	-6.7	758.4	170.6	5351.3	-9.9
1.10	34.9	-10.2	747.7	167.7	5383.5	-12.3

Table 2: Listed are estimated Volterra kernels at different frequencies for f_1 using Method 2.

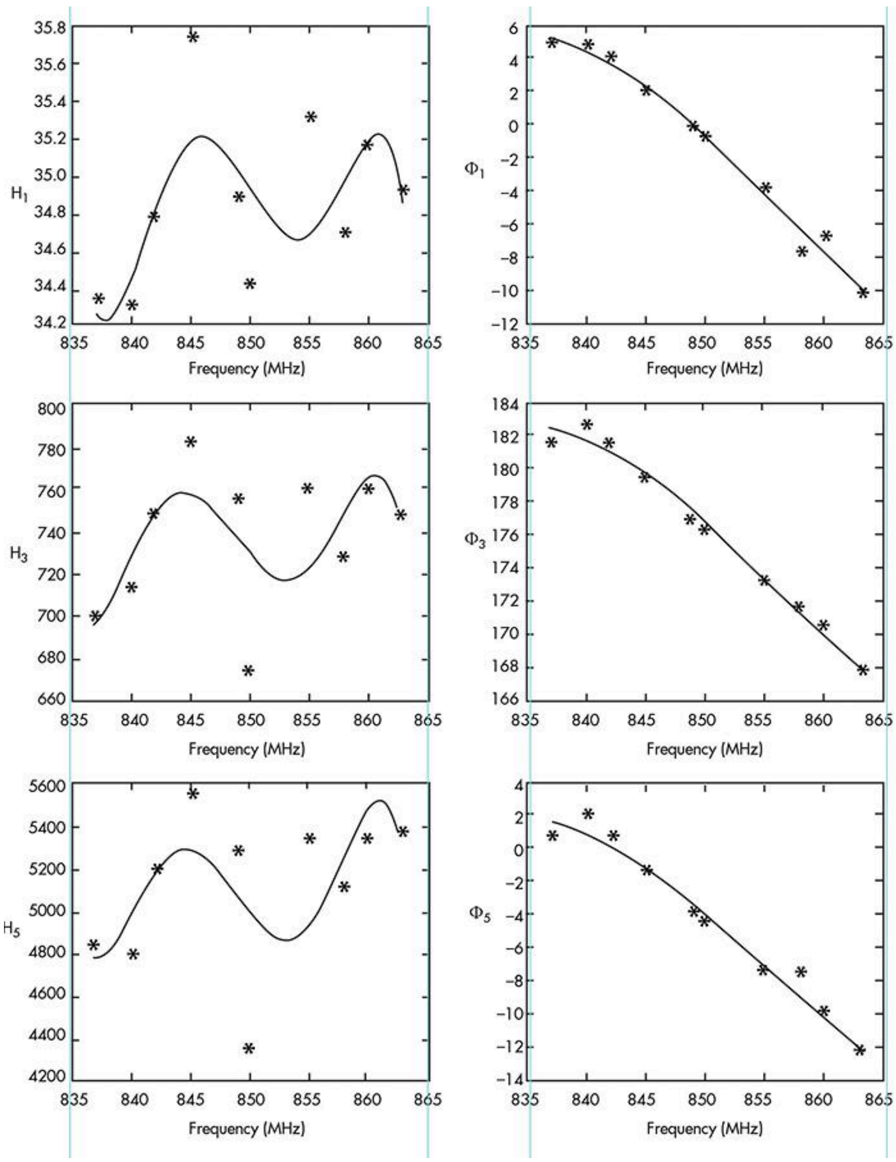

10. Using Method II, the estimated Volterra kernels are given at different frequencies, as is the frequency dependency of kernels for the bandwidth of 837 to 863 MHz.

As *Table 2* and *Figure 10* show, H_1 is almost constant—it only varies between 34.3 and 35.7. The variation of H_3 is larger (between 670 and 790), while the largest variation occurs with H_5 (between 4,300 and 5,600).

METHOD 1 MEASUREMENTS

According to Method 1, to estimate the Volterra kernels $H_1(f)$, $H_3(f)$, and $H_5(f)$, it's required to determine three points (P_{in}, P_{out}) on the power curve and three points (P_{in}, Φ_{out}) on the phase curve for the frequency f_1.

Table 1 shows the estimated Volterra kernels at different frequencies for f_1 according to Method 1. *Table 1* and *Figure 7* show how the different components of the Volterra kernels vary with frequency.

We can see that H_1 is almost constant—it only varies between 35.3 and 36.9. On the other hand, H_3 varies more—somewhere between 700 and 1,100. The greatest variation is seen in H_5, which varies between 1,500 and 8,000. The angles φ_1 and φ_3 are almost linear, whereas φ_5 varies strongly. To estimate frequency dependency of the Volterra kernel within the bandwidth of 837 to 863 MHz, the estimated values from *Table 1* were adapted in the following equations:

$$
\begin{aligned}
H_1 =& 2.89\cdot10^{-7}f_5 - 1.17\cdot10^{-3}f_4 + 1.88f_3 - \\
& 1.51\cdot10^{3}f_2 + 6.04\cdot10^{5}f - 9.63\cdot10^{7} \\
\phi_1 =& 8.51\cdot10^{-4}f_3 - 2.18f_2 + 1.86\cdot10^{3}f - 5.28\cdot10^{5} \\
H_3 =& 8.86\cdot10^{-4}f_5 - 3.76f_4 + 6.38\cdot10^{3}f_3 - \\
& 5.41\cdot10^{6}f_2 + 2.30\cdot10^{9}f - 3.90\cdot10^{11} \\
\phi_3 =& 2.84\cdot10^{-3}f_3 - 7.23f_2 + 6.14\cdot10^{3}f - 1.74\cdot10^{6} \\
H_5 =& -1.30\cdot10^{-2}f_5 + 5.50\cdot10^{1}f_4 - 9.36\cdot10^{4}f_3 + \\
& 7.97\cdot10^{7}f_2 - 3.39\cdot10^{10}f + 5.77\cdot10^{12} \\
\phi_5 =& -1.29\cdot10^{-3}f_4 + 4.34f_3 - 5.50\cdot10^{3}f_2 + 3.09\times10^{6}\cdot f - 6.52\times10^{8}
\end{aligned}
\tag{32}
$$

Figure 7 shows the result of these adaptations. We can see that the adaptation of H_1, H_3, H_5, and φ_5 is not precise. It's likely that more precise results could be obtained by spending more time selecting the points. To determine the accuracy of the estimated results, we can compare these results to the broadband measurements.

From Equation 5, it's possible to determine other frequencies (f_3, f_4, f_5, and f_6) when the two-tone frequencies, f_1 and f_2, are applied to the amplifier. Now, by substituting these frequencies in Equation 32, we can obtain kernel values for these frequencies. Substituting these values in Equation 5 gives us the calculated output. Finally, after all calculations are performed, we obtain the results *(Figs. 8 and 9)*.

In both cases, the calculated and measured power curves for f_1 and f_3 are perfectly matched up to input power levels of –10 dBm *(Figs. 8a and 9a, again)*. *Figure 8b* reveals that the difference between the calculated and measured angles is about 2 to 3 degrees up to input power levels of –9 dBm. However, at input power levels greater than –9 dBm, the calculated angles deviate significantly from the measured values. For the other measurement, the difference between the calculated and measured angles is very small up to input power levels of –8 dBm *(Fig. 9b)*. However, the difference starts to increase for input power levels beyond –8 dBm.

METHOD 2 MEASUREMENTS

Next, 30 narrowband measurements for both the power curve (P_{in}, P_{out}) and the phase curve (P_{in}, φ_{out}) were performed. These values are applied to estimate the Volterra kernels, $H_1(f)$, $H_3(f)$, and $H_5(f)$, according to equation (28). *Table 2* shows the estimated Volterra kernels.

As *Table 2* and *Figure 10* show, H_1 is almost constant—it only varies between 34.3 and 35.7. The variation of H_3 is larger (between 670 and 790), while the largest variation occurs with H_5 (between 4,300 and 5,600). All three angles variations behave almost linearly with the difference between the highest and lowest angles being 15 degrees. To estimate frequency dependency of the Volterra kernel within the bandwidth of 837 to 863 MHz, the estimated values from *Table 2* were utilized in the following equations:

$$
\begin{aligned}
H_1 =& -9.31\cdot10^{-6}f_5 + 3.96\cdot10^{-2}f_4 - 6.72\cdot10^{1}f_3 + \\
& 5.71\cdot10^{4}f_2 - 2.43\cdot10^{7}f + 4.12\cdot10^{9} \\
\phi_1 =& 5.52\cdot10^{-4}f_3 - 1.42f_2 + 1.21\cdot10^{3}f - 3.45\cdot10^{5} \\
H_3 =& -5.10\cdot10^{-4}f_5 + 2.16f_4 - 3.67\cdot10^{3}f_3 + \\
& 3.12\cdot10^{6}f_2 - 1.32\cdot10^{9}f + 2.24\cdot10^{11} \\
\phi_3 =& 6.22\cdot10^{-4}f_3 - 1.60f_2 + 1.36\cdot10^{3}f - 3.88\cdot10^{5} \\
H_5 =& -6.08\cdot10^{-3}f_5 + 2.58\cdot10^{1}f_4 - 4.38\cdot10^{4}f_3 + \\
& 3.72\cdot10^{7}f_2 - 1.58\cdot10^{10}f + 2.68\cdot10^{12} \\
\phi_5 =& 5.10\cdot10^{-4}f_3 - 1.31f_2 + 1.12\cdot10^{3}f - 3.18\cdot10^{5}
\end{aligned}
\tag{33}
$$

Figure 10 shows the result of these adaptations. For the adaptation, the highest polynomial of grade five is applied. Like Method 1, the adaptation did not work precisely. It's probable that estimating the higher-order Volterra kernels would lead to more precise results. Here, the accuracy of the estimated results is again determined by comparing them to the broadband measurements *(Figs. 11 and 12)*. The power curves show a good estimation for f_1 up to input power levels of –2.5 dBm *(Figs. 11a and 12a, again)*. However, at higher input power levels, the calculated values differ.

The calculated power curve for f_3 is precise up to input power levels of –8 dBm. If a difference of up to 5 dB between the calculated and measured power curves for f_3 was admissible, the calculated f_3 up to an input power level of –2.5 dBm could be acceptable. *Figure 11b* reveals that the difference between the calculated and measured angles of f_1 up to input power levels of +2.5 dBm is as high as 5 degrees. Furthermore, *Figure 12b* shows similar results for the other case.

The calculated power curve for f_3 is precise up to input power levels of –8 dBm. If a difference of up to 5 dB between the calculated and measured power curves for f_3 was admissible, the calculated f_3 up to an input power level of –2.5 dBm could be acceptable.

CONCLUSION

This article presented two methods to estimate Volterra kernels by measuring power values in a specific frequency

This article presented two methods to estimate Volterra kernels by measuring power values in a specific frequency band and drawing power curves to determine the best points to formulate and calculate Volterra kernels. To demonstrate the efficiency and accuracy of the methods discussed, experiments were performed using an RF amplifier, the ZFL-1000H from Mini-Circuits.

band and drawing power curves to determine the best points to formulate and calculate Volterra kernels. To demonstrate the efficiency and accuracy of the methods discussed, experiments were performed using an RF amplifier, the ZFL-1000H from Mini-Circuits. To assess the effectiveness of these methods, the outputs were calculated through the estimated kernels and the Volterra series for some specific inputs. The results were then compared with the measured outputs.

In Method 1, points (P_{in}, P_{out}) and (P_{in}, φ_{out}) were used to estimate the kernel values. The procedure for determining which points to use consist of studying the measured power curves, guessing, and testing.

In Method 2, the polynomial adaptation of measured power and phase curves were performed. Then, from these adaptation results, i.e., the coefficients of the polynomials, the kernel values were estimated. A comparison of these two methods

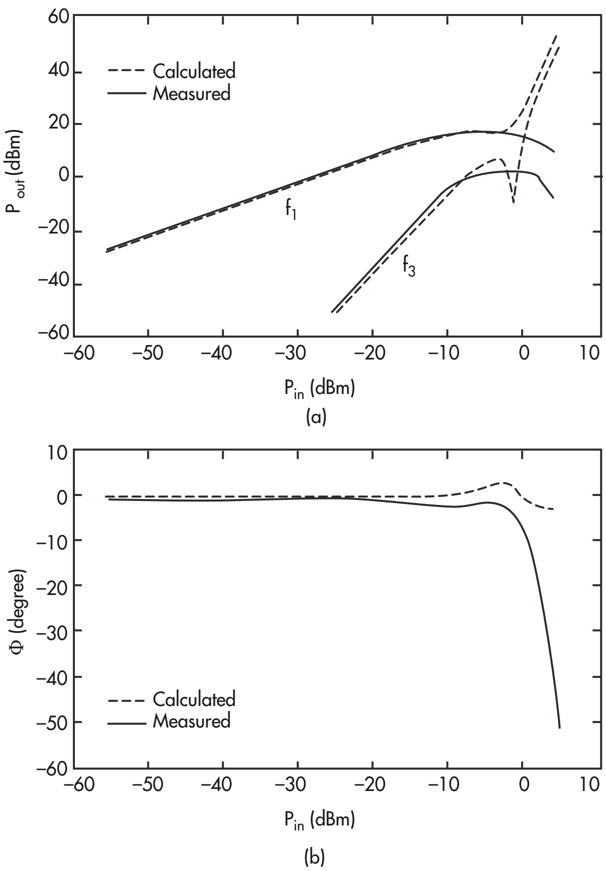

11. In this broadband measurement, f_1 = 850 MHz and f_3 = 847 MHz. Shown are measured and calculated $P_{out}(P_{in})$ curves at frequencies f_1 and f_3 (a), and measured and calculated angles of f_1 (b).

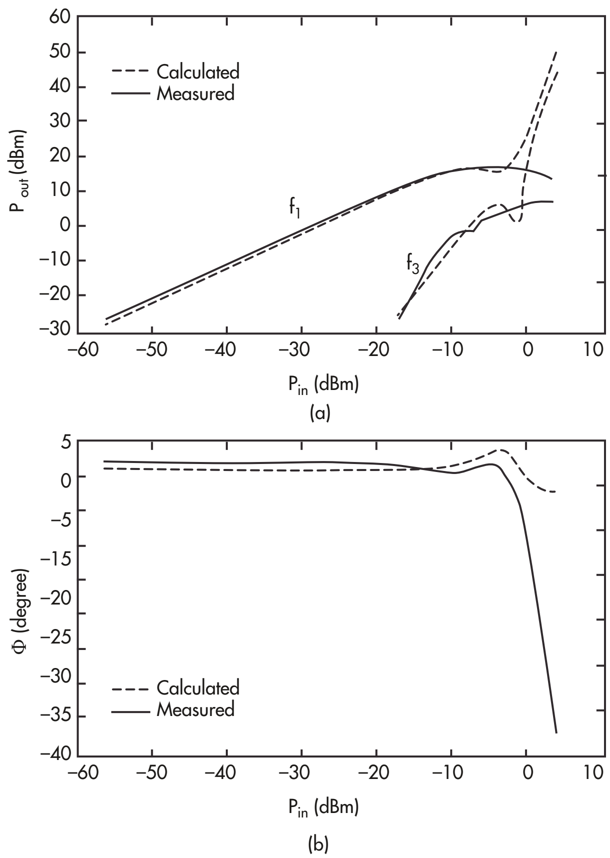

12. In this broadband measurement, f_1 = 847 MHz and f_3 = 842 MHz. Shown are measured and calculated $P_{out}(P_{in})$ curves at frequencies f_1 and f_3 (a), and measured and calculated angles of f_1 (b).

> In Method 1, by spending more time selecting the points and using these points in relation to the amplifier's compression point or intercept point, it's possible to use these points for any other amplifier. In Method 2, it's possible to estimate the higher-order Volterra kernels by increasing the degree of the adaptation polynomials, which is usually difficult to perform.

revealed that Method 2 provides better results. In addition, Method 2 is easier and faster to perform.

Further research can be carried out to improve and develop these two methods. In Method 1, by spending more time selecting the points and using these points in relation to the amplifier's compression point or intercept point, it's possible to use these points for any other amplifier. In Method 2, it's possible to estimate the higher-order Volterra kernels by increasing the degree of the adaptation polynomials, which is usually difficult to perform. In other words, the numerical problems may arise in the polynomial adaptation. mw

REFERENCES

1. S. Ghadimi and T. Larsson, "Bestämning av Volterra-kärnor f'or HF effekt förstärkare," Master's thesis, Lund University, Lund, Sweden, 1995.
2. M. Johansson, "Linearization of wide-band RF power amplifiers using modulation feedback," Ph.D. dissertation, Lund University, Lund, Sweden, Nov. 1995, IUTEDX/(TETE-1012)/1-65.
3. Y. Kuo, "Frequency-domain analysis of weakly nonlinear networks," Circuits and Systems, vol. 11, no. 4, pp. 2-8, Aug 1997.
4. G. Einarsson, Olinijära system representerade med Volterra serier. Lund, Sweden: Lund University, 1971.
5. J. G. McRory and R. Johnson, "Volterra kernel estimation for mildly nonlinear amplifiers," *Electronics Letters*, vol. 29, no. 23, pp. 2007–2008, Nov 1993.
6. T. T. Ha, *Solid-State Microwave Amplifier Design*. New Jersey: Wiley, 1981.
7. S. Boyd, Y. Tang, and L. Chua, "Measuring volterra kernels," *IEEE Transactions on Circuits and Systems*, vol. 30, no. 8, pp. 571–577, Aug 1983.

FARRON DACUS | RF Design Consultant, Longwing Technology
www.longwingtech.com

Key Parts for Ultra-Low-Noise Synthesizer Design

The focus in this article is on the key parts needed for ultra-low-noise synthesizer design like crystal references, power supplies, and low-noise op amps.

Welcome to Part 4 of this 5-part series on ultra-low-noise synthesizer design. Part 1 introduced advanced loop design and included both passive and active filters. Part 2 covered noise sources in the loop outside of the synthesizer integrated circuit (IC). Part 3 added synthesizer IC noises and how they are modeled, as well as how all of the noise sources are combined and shaped by the loop.

This article covers the key parts required by design engineers seeking the lowest-noise designs, or lowest noise for a particular cost. Since the designer is naturally concerned with the cost tradeoffs of these key parts, that information is presented in some detail here. Additional information is available in the long version posted on the Longwing Technology website *(www.longwingtech.com)*. Part 5 will bring it all together in the form of low-noise examples, comparing and contrasting the performance attained by the various methods and the available parts.

KEY COMPONENTS

Major Trends

The most significant trend driving lower noise in modern single-loop synthesizers is the development of the delta-sigma synthesizer IC in very high-speed IC processes. This synthesizer approach allows for fractional-N synthesis with real number multiplication of the reference frequency. A key breakthrough is that high fractional resolution allows for high-frequency references. This, in turn, enables high bandwidth for maximum noise suppression inside a much wider loop bandwidth than integer synthesizers allow for, i.e., bandwidths may now exceed 400 kHz.

Another important factor is associated with using multiple voltage-controlled oscillators (VCOs) on die combined with hundreds of narrowband resonators (Ref. 5). In this scenario, which emulates wideband VCOs to hit any frequency by use of frequency division, the on-die noise performance past the loop bandwidth in offset and above about 4 GHz in VCO frequency can generally match or beat the best octave-bandwidth discrete VCOs.

The best octave-bandwidth VCOs below 4 GHz can currently outperform on-die narrowband emulations of wideband VCOs by about 2 to 8 dB, while the best narrowband VCOs can exceed on-die performance by 10 to 30 dB. It's thus mostly in the narrowband VCO case, and in applications in which noise past the loop bandwidth of typically about 50 to 400 kHz is critical, where discrete VCOs still find success.

Integer-N synthesizer crystal references in the past were usually in the range of 1 to 20 MHz (10 MHz being a popular choice), with divided frequency steps typically in the range of 1 to 200 kHz as per system requirements. However, the capability of the fractional-N synthesizer to effectively hit any frequency with only small error allows for the use of higher-frequency references.

Crystal oscillators as high as 100 MHz are now becoming available at cost-effective prices, and many synthesizers enable internal doubling to 200 MHz to allow for even higher loop bandwidths. The need to support ultra-low-noise VCOs and crystal oscillators also led to lower-noise voltage regulators to supply them.

SYNTHESIZER ICs

Among the key issues associated with choosing modern delta-sigma synthesizers are internal noise parameters, which model the noise that the charge pump and dividers induce on the VCO in the closed-loop state. These are further described in the long form of this article, and in still more detail in Part 3 of this series (Ref. 3). The parameters are modeled as a flat and 1/f noise term for each part.

When using a device in fractional mode, the in-band phase noise may be slightly degraded, depending on the fraction and how it's expressed. This fractional noise floor appears to add to the integer noise floor modeled by the term PN1Hz. Some manufacturers, such as Analog Devices (ADI) *(www.analog.com)*, may account for this by increasing PN1Hz by a modest amount, which may be 1 to 3 dB in fractional mode.

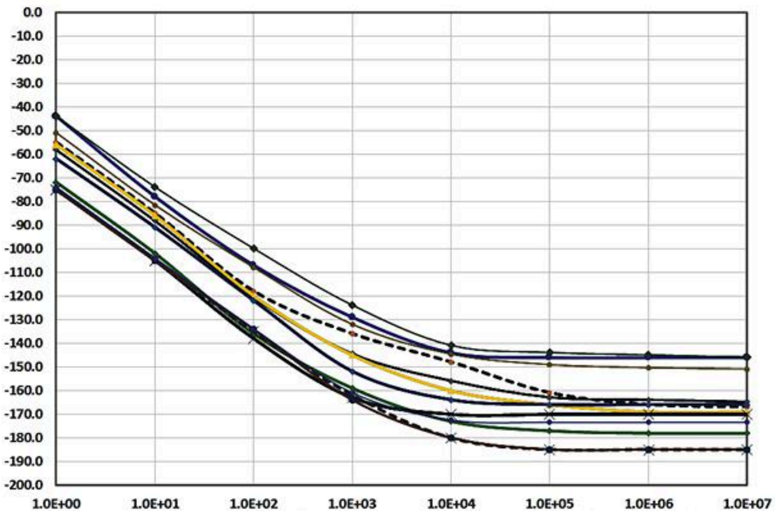

1. Shown are example phase noises for crystal oscillators displaying excellent noise performance. These commercially available parts operate from 28 to 100 MHz; here, they are normalized to 100-MHz noise performance for fair comparison.

TABLE 1: SYNTHESIZER ICs

Part	Freq range	On-die VCO	Norm phase-noise floor and flicker in dB, and total noise figure of merit	Price	Comments
TI LMX2491	500 MHz to 6.4 GHz	No, only ext	–227 floor dB –260 flicker dB 1.35E-17 tot	$2.90 @1k	State of the art for the price. FMCW radar functions. Charge pump can tune to 5.25 V. The LTC6947 is a similar competitor, but about 2X the cost. The LMX2492 is a 14-GHz version for ~$8.75 @ 1k.
TI LMX2571	10 MHz to 1344 MHz Internal VCO, 100 MHz to 2 GHz External VCO	Yes, option for off-die	–231 floor –260 flicker 1.23E-17 tot	$5.50 @1k	State-of-the-art lower power synthesizer. Ext VCO to 2 GHz, but RF buffer output limited to 1400 MHz. This part is ideally architected for land mobile use.
TI LMX2572LP	12.5 MHz to 2 GHz	Yes	–232 floor –265.5 flicker 5.77E-18 tot	$6 @1k	State-of-the-art lower power, lower freq, lower cost synthesizer.
TI LMX2582	20 MHz to 5.5 GHz	Yes	–231 floor –266 flicker 3.67E-18	$9 @1k	State of the art for the price in a medium frequency. The LMX2592 is a 9.8-GHz version for $20.50 @ 1k.
TI LMX2594	10 MHz to 15 GHz	Yes	–236 floor –269 flicker 1.7E-18 tot	$42.50 @1k	State-of-the-art on-die VCO synth IC. The -235dBc/Hz normalized frac PLL noise is the lowest currently available. The LMX2595 is a 20-GHz version for $62.50 @ 1k.
Analog Devices ADF41513	1 GHz to 26.5 GHz	No, ext. only	–234 int floor –231 frac floor –267 flicker 3.09E-18 tot	~$30 @1k	State of the art for a high-frequency ext. VCO synthesizer. The –231-dBc/Hz fractional normalized PLL noise is the lowest currently available for external VCOs.
Analog Devices ADF4372	62 MHz to 16 GHz	Yes	–234 int floor –233 frac floor –267 flicker 2.3E-18 tot	~$65 @1k	Near state of the art, though LMX2594 is a direct competitor with lower noise and cost. Typical spurious of –90 dBc. The ADF4371 is a 32-GHz version at ~$250 @ 1k.
Analog Devices ADF5610	57 MHz to 14.6 GHz	Yes	–232 int floor –229 frac floor –268 flicker 2.46E-18 tot	~$48 @ 1k	Near state of the art at a lower price than the ADF4372, with low typical spurs of –105 dBc, at the cost of about 4 dB higher in-band phase noise.

Listed are leading delta-sigma synthesizer ICs. Lower noise is more expensive, but lower noise combined with higher frequency is what really costs. Note: Texas Instruments reports no difference in broadband phase noise between integer and fractional mode, though spurs may vary. Analog Devices typically reports a difference in integer and fractional mode normalized noise, in which fractional is about 1 to 3 dB noisier.

In Part 3, a figure of merit combining the noises of the flat and 1/f terms is developed. Results of this combination are shown in *Table 1*. This figure of merit is proportional to synthesizer-chip-induced noise power from 1 Hz to a bandwidth of fL. Therefore, smaller is better.

CRYSTAL REFERENCES

In the case of the modern delta-sigma, fractional-N, high-bandwidth synthesizer, the crystal reference oscillator is the component that can often be the most expensive and have the greatest impact in the system. Phase noise is considered at offsets from the carrier on a per-Hz basis. Inside the loop bandwidth, there will typically be a range of frequencies in which the synthesizer-chip noise parameters set the phase-noise floor, as well as a lower range of frequencies in which the multiplied crystal oscillator noise is dominant over the chip noise. Understanding the tradeoffs here can significantly affect the total cost.

Figure 1 shows the phase-noise performance of a set of commercially available crystal reference oscillators that, under different conditions, are all well-suited for modern usage. Though these are all low-noise oscillators for their price, there's a phase-noise variation of approximately 30 to 40 dB. Even more striking is the price variation, which varies from less than $2 to over $1,000.

For decades, 10 MHz was the standard frequency of the finest low-noise crystal oscillators. However, 100 MHz is rapidly becoming a new standard for this application, with both voltage-controlled temperature-compensated crystal oscillators (VCTCXOs) and ovenized oscillators now available. Lower-cost simple crystal oscillators will typically have 10 to 100 parts per million (ppm) accuracy and temperature drift. This performance, if acceptable, can lead to quite good noise performance for prices ranging from less than $2 to about $12.

VCTCXOs offer frequency accuracy from about 0.5 to 2 ppm. VCTCXOs at frequencies under 40 MHz with phase noise suitable for wireless handsets (typi-

TABLE 2: CRYSTAL REFERENCES

General requirements	Part	Freq	Accuracy and phase noise @ 1 kHz norm to 100 MHz	Typical cost	Comments
Low-cost VCTCXO	Taitien TY	40 MHz	±1 ppm –124dBc/Hz	~$0.80 to $1.80	Excellent performance for a low-cost handset class VCTCXO.
Lost cost and relaxed accuracy up to 50 MHz	Mercury HJ XO series	20 to 50 MHz	25-, 50-, and 100-ppm total error, including temp. –135 dBc/Hz.	~$1.3 - $2.90	Outstanding noise for the price. Mercury reports they can offer these parts at ±5- and ±10-ppm accuracy at 25°C. That implies max temp drift over –40 to +85°C, aging, and supply can be limited to 18 ppm. Standard CMOS output.
Lost cost and relaxed accuracy up to 160 MHz	Abracon ABLNO XO series	24.576 to 160 MHz	±12 ppm typ at room temp, additional +6/–8 ppm over –30 to +85°C. –143 dBc/Hz.	~$8 - $12	Outstanding noise for the price, if accuracy is acceptable. 28-ppm max total error, 18-ppm max temp drift, 7-ppm aging => set on accuracy of 3 ppm. Nom freq error over –40 to +85°C and 10 years aging is thus 22 ppm.
High-performance VCTCXO	Taitien TKCAB	100 MHz	±1 ppm at 25°C and ±1 ppm over temp. –145 dBc/Hz	~$30 to $45	A new breakthough VCTCXO within 5 to 7 dB of the noise of low-end ovenized oscillators for about 1/3 the price.
High-performance VCTCXO	NEL AN-X0AU AN-XA7XU	60 to 128 MHz, nom 100 MHz	Grades ranging from ±0.28 to ±25 ppm, –155 to –160 dBc/Hz	Not public	High-performance VCTCXO that competes with ovenized oscillators for generally less cost and much less power.
Low-end ovenized	Taitien 2900 series	100 MHz	±0.2 ppm at 25°C and 50 ppb over temperature. –152 dBc/Hz	~$80 to $110	An excellent representative of the lower end of ovenized references, with outstanding accuracy.
Mid-grade ovenized	KVG LPN series	80 to 150 MHz, nom 100 MHz	±-0.3 ppm at 25°C 20 to 200 ppb over temp and grade. –163 dBc/Hz max	~$350 @ 100 ~$285 @ 1k	Superior noise performance for mid-grade ovenized. Options are available from "A" to "D" that trade close in noise against far out noise. Opt D pricing is shown here.
High-end ovenized	KVG ULPN series	100 MHz	±0.3 ppm at 25°C 50 to 500 ppb over temp and grade. -164 dBc/Hz max	$500 to $750 @ 1k over grade	High-grade performance at the low end of high-grade pricing. Grades P1, P2, and P3 are available.
High-end ovenized	NEL O-CIH	100 MHz	50 ppb over temp –158 to –166 dBc/Hz over grade	Not public	State of the art in the higher grades.

Listed are strong crystal oscillator candidates for low-noise synthesizers. Costs reflect moderate to medium volume for the typical applications of the part, and in some cases are estimated by the author.

cally consuming less than 3 mA) are available for less than $2 and sometimes less than $1 in high volumes. At 40 MHz and with performance suitable for base stations, price ranges from about $4 to $8.

However, newly released VCTCXOs at 100 MHz (Taitien, *www.taitien.com*, TKCAB) that are ideal for the latest synthesizer ICs aimed at high-performance communications, wireless infrastructure, and test equipment are tending to be in the price range of $25 to $40. For the most demanding applications, ovenized oscillators at 100 MHz with initial frequency accuracy from 0.2 to 0.5 ppm and very well-controlled aging and temperature drift range cost about $70 to $1500. However, outstanding performance can be obtained by the careful designer for about $250 to $500. The price-performance ratios may be visualized by *Figure 2*.

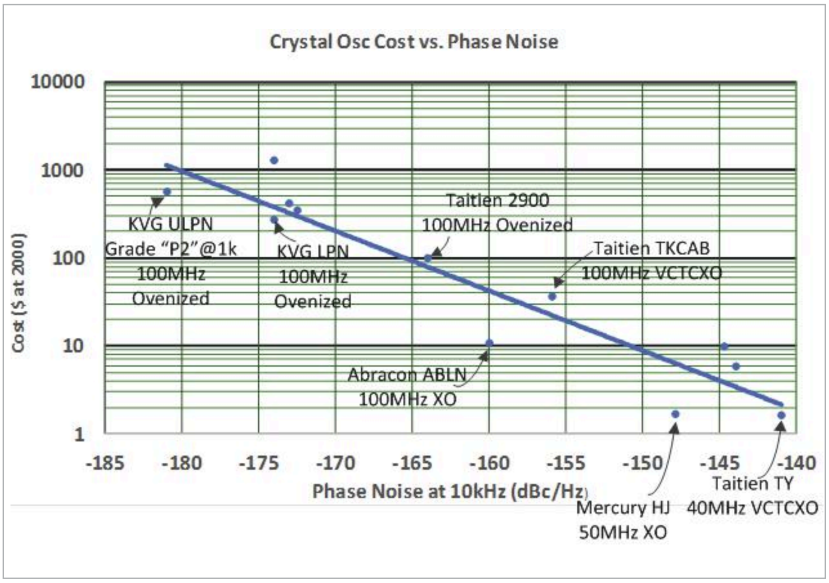

2. This approximate price-versus-noise-performance graph of well-performing crystal oscillators, with trend line curve fit, gives a designer a quick view in terms of what must be spent to obtain certain phase-noise performance.

TABLE 3: VCOs

Part	Freq	Phase noise @ 10 kHz and 100 kHz, dBc/Hz	Tune and supply	Comments
Synergy DCRO178205-10	1785 to 2060 MHz	–109, –131	0.5 to 12 V 10 V @ 35 mA	Near the limit of available for a 2-GHz part with ±7% tune range. About 13 dB better noise than the best on-die VCO performance such as that on the LMX2495.
Synergy DCYS100200-12	1 to 2 GHz	–106, –128 (some variation over this wide band)	0.5 to 28 V 12 V @ 40 mA	Superb for a microwave octave tune range that with on-synthesizer dividers can hit any frequency from HF to 2 GHz. About 8 dB superior to a state-of-the-art on-die VCO.
Synergy DCYS200400P-5	2 to 4 GHz	–93, –116	0.5 to 18 V 5 V @ 60 mA	Excellent for an octave at this frequency, though on a normalized basis about 6 dB inferior to DCYS100200-12. About 2 dB superior to a state-of-the-art on-die VCO such as that on the LMX2495. Above 4 GHz, it's difficult to find octave VCOs that are significantly better than the best integrated.
Mini-Circuits MOS-975-119+	900 to 975 MHz	–114, –135	1 to 9 V 5 V @ 40 mA	Excellent for the ±-4% tune range, effectively –120 if divided by 2 to land mobile band. About 11 dB superior to best on-die VCOs. $15.75 @ 100.
Mini-Circuits ROS-1770-1PH19+	1710 to 1800 MHz	–111, –132	0.5 to 8 V 5 V @ 30 mA	Excellent for its ±2.6% tune range, effectively –123 divided by 4 to land mobile. About 13 dB superior to best on-die VCOs. $19.95 @ 100.
Mini-Circuits ROS-2001C-119+	2 GHz (1997 to 2003 MHz)	–126, –147	0.5 to 9.5 V 8 V @ 38 mA	Excellent for pure performance at 2 GHz, even though a point frequency product. About 29 dB better than best on-die VCOs. $39.95 @ 50.
Z-Comm ZRO0915C2LF	902 to 928 MHz	–128, –147	0 to 11 V 10 V @ 23 mA	Superb for 902- to 928-MHz low-noise apps such as RFID readers. About 23 dB better than best on-die performance. Budgetary pricing ~$19 for 1k and $13 for 10k.
Analog Devices HMC510	8.45 to 9.55 GHz	–92, –116	2 to 13 V 5 V @ 315 mA	Excellent noise in this narrowband family for frequencies in the range of 8 to 27 GHz. This particular VCO is about 11 dB better than the best on-die VCOs at 100 kHz, and others in this family in the range of 8 to 12 dB better. These have div-by-2 outputs and some also div-by-4 in order to use lower-cost, lower-frequency synthesizer ICs. $22.55 at 50.

These are noteworthy VCO candidates for low-noise synthesizers. While noise well inside the PLL bandwidth will be similar to that of integrated VCOs, these parts can provide significantly lower phase noise around and past the loop bandwidth.

This dB linear graph shows that the general cost versus phase-noise function is an approximate hyperbola, which is quantified and discussed in more depth in the long version at *www.longwingtech.com*. The main takeaway is that there's a predictable relationship here to help the designer understand a fair market price for the specifications needed. More details of examples of good performance-price ratio crystal oscillators are reviewed in *Table 2*.

CRYSTAL-REFERENCE DRIVE AND BUFFERING

This subject is insufficiently reported on, and often more difficult than it seems at first glance. These synthesizer inputs have demanding slew-rate requirements for best noise performance, may have matching requirements, and often have some surprising voltage requirements. A voltage peak-to-peak swing above a minimum is needed, but usually also with a maximum that's less than the synthesizer chip supply rails. This is reviewed in some depth in the long version at *www.longwingtech.com* with recommended buffer parts.

There's a disconnect here in the market between optimum drive for different synthesizers and what crystal oscillators typically provide; therefore, users may have to provide their own buffering.

There's a disconnect here in the market between optimum drive for different synthesizers and what crystal oscillators typically provide; therefore, users may have to provide their own buffering. It's a surprisingly important issue, as phase-noise degradation exceeding 10 dB can occur.

DISCRETE VCOs

Low-noise VCOs have historically been provided as modules by companies that were specialists in pushing Leeson's Equation (Ref. 2) to the limits of physics and parts, which required high-Q resonators and a detailed understanding of all noise sources in a VCO. To remain relevant with on-die VCOs taking an ever-increasing market share, new even lower-noise VCOs have continued to come out. Such products include the narrowband VCOs offered by Mini-Circuits *(www.minicircuits.com)*, Synergy Microwave *(www.synergymwave.com)*, Z-Comm *(www.zcomm.com)*, and Analog Devices.

The best narrowband VCOs have about 10- to 30-dB better noise performance than the best on-die VCOs. Synergy Microwave, with its metamaterial resonator VCOs, offers octave-bandwidth VCOs to about 4 GHz with phase noise that's within about 5 to 20 dB of the very best narrowband VCOs at similar frequencies, and typically about 2 to 8 dB superior than the finest on-die VCOs. Though on-die VCOs are probably taking over 80% of design-ins, high-performance discrete VCOs are still finding application in microwave links, test equipment, military communications, and wireless infrastructure. Some key examples are given in *Table 3*.

POWER SUPPLIES

Low-noise regulators represent an area of important recent advancement. Noise on supplies will directly modulate noise on a VCO, as described in Part 2 of this series. As recently as 2010, a noise floor of about 10 to 30 nV per root Hz was considered "ultra-low noise." These levels could induce considerable degradation of the phase noise of a low-noise VCO.

For this reason, the author had previously designed custom discrete regulators with floor of 1 nV or lower when such performance was needed. In 2015, noises as low as 2 nV were introduced to the market by Linear Technology in very convenient form. For the majority of applications, a supply noise level of 2 nV per root Hz eliminates supply noise as a practical concern.

Regulator noises for four top options are shown in *Figure 3*. In the author's opinion, the most usable low-noise regulator on the market is the 2-nV-floor LT3042 from Linear Technology (now Analog Devices). It provides voltages of 0 to 15 V at up to 200-mA output. The new LT3045 provides up to 500 mA. In addition, the recently introduced LT3093 and LT3094 deliver similar performance in negative voltage regulator form. *Table 4* shows key specifications of several top low-noise regulator choices.

LOW-NOISE OP AMPS

Op amps are needed to boost charge-pump outputs to the higher voltages required to tune the very finest discrete VCOs. However, their noise will directly modulate noise onto the VCO output and must be very low to be transparent (Ref. 2). Op amps with noise floors approaching 1 nV have been available for many years. In recent years, though, these op amps have improved with lower input current (important for low spurs) and current noise (also very important), greater common-mode range, and higher bandwidth (important to spurs and phase shift).

However, the very lowest-noise op amps are not rail to rail, and care must be taken when locking the phase-locked loop (PLL) using these op amps. Typical methods of working with non-rail-to-rail op amps are to make use of a low-noise negative supply for the op amp, pre-charge the loop filter under software control to be within the input voltage range of the op amp, or switch in a rail-to-rail op amp during initial settling. Table 5 lists low-noise op amps for use in low-noise synthesizers.

SUMMARY

Delta-sigma synthesizer ICs with on-die VCOs and output dividers have reshaped the design of synthesizers in the last decade. Available at frequencies as high as 32 GHz, they can typically provide any output frequency from a few tens of MHz to their upper frequency limit. The inherent higher phase noise of on-die VCOs has been partially tamed by switching VCOs and resonators for the best open-loop on-die VCO phase noise, and then suppressing that noise with high-frequency crystal oscillators and higher phase-detector frequencies to allow for higher loop bandwidths out to approximately 200 to 400 kHz.

Discrete-VCO-based synthesizers can still offer the advantage of superior phase noise around and past the loop bandwidth. For the best narrowband and point frequency VCOs, this advantage is quite significant (about 20 to 30 dB). For octave-bandwidth VCOs that offer similar frequency flexibility to on-die VCOs, the advantage is more limited—about 2 to 8 dB for VCOs under 4 GHz.

The discrete VCO approach currently pays a penalty of moderately higher noise (approximately 3 to 4 dB) over part of the range within the loop bandwidth due to the best PLL noise (charge pump and divider noise) being available only for VCO on-die synthesizers and not for synthesizers supporting external VCOs. The discrete VCO approach also requires extra parts for higher voltage supplies and active loop filters. Still, in markets like test equipment, microwave links, wireless infrastructure, and low-noise communications, there are places for the discrete VCO approach. Examples will be shown in the concluding fifth article of this series.

THE AUTHOR wishes to express his appreciation for the information and reviews provided by Dean Banerjee at Texas Instruments, Marty Richardson at Analog Devices, Miguel Troester and C.Y. Teng at Taitien, Harald Rudolf at KVG Quartz Crystal Technology, and Daniel Loomis at Z-Communications.

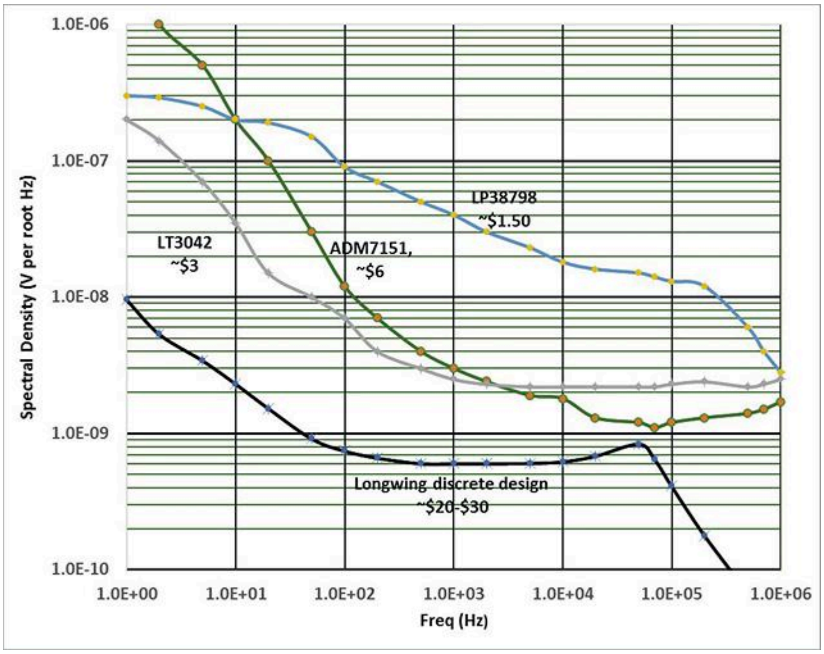

3. Ultra-low-noise regulator spectral noise density is compared in this plot. The LT3042 and ADM7151 noise curves were both obtained with 22-μF noise-filter capacitances.

TABLE 4: REGULATORS

Regulator	Key specs	Cost and comments
TI LP38798	V_{in}: 3 to 20 V V_{out}: 1.2 to V_{in}-dropout Current limit: 800 mA Dropout: 200 mV Thermal resistance: ~35°C/W	~$1.50 at 2k distributor. Noise is first-order independent of output voltage. The low-cost choice for a low-noise, high-current, high-voltage regulator.
Linear LT3042 (200 mA) LT3045 (500 mA) LT3093 (200 mA neg) LT3094 (500 mA neg)	V_{in}: 1.8 to 20 V V_{out} : 0 to 15 V Current limit: 200 mA Dropout: 350 mV thermal Resistance: ~33°C/W	~$2.85 at 2500 distributor. Noise is first-order independent of output voltage. The ultra-low-noise choice for wide voltage range, offering positive and negative outputs.

Listed are key specifications of several top low-noise regulator choices.

REFERENCES

1. "Design Methods of Modern Ultra-Low Noise Synthesizers," Farron Dacus, *Microwaves & RF*, Dec. 2018.
2. "Noise Sources in Ultra-Low-Noise Synthesizer Design," Farron Dacus, *Microwaves & RF*, Feb. 2019.
3. "Noise and its Shaping in Ultra-Low-Noise Synthesizer Design," Farron Dacus, *Microwaves & RF*, Mar. 2019. Long forms of these articles with more detail are posted at www.longwingtech.com.
4. "Supply clean power with ultra-low-noise LDO regulators," Steve Knoth, https://www.electronicproducts.com/Power_Products/Power_and_Control/Supply_clean_power_with_ultra_low_noise_LDO_regulators.aspx.
5. "A 2-to-16GHz BiCMOS ΔΣ Fractional-N PLL Synthesizer with Integrated VCO's and Frequency Doubler for Wireless Backhaul Applications," Tino Copani et. al., STMicroelectronics, 2016 ISSCC. Available from the IEEE.

TABLE 5: OP AMPS

Op amp	Major specs	Cost and comments
TI OPA209 single and OPA2209 dual	Rail-to-rail output, 1.5-V drop on input. Voltage noise 8.1(1 Hz)-3.3-2.3-2.2-2.2 nV. Current noise 1.6 pA (1 Hz)- 0.6-0.5-0.5. Supply 4.5 to 36 V. Input bias 1 to 8 nA. 18-MHz GBW.	Single $1.10 @ 1k Dual $1.65 @ 1k Lower input bias and noise current than most ultra-low-noise op amps can sometimes enable, outperforming op amps with lower voltage noise.
TI OPA1611 single and OPA1612 dual	Output rail to rail, input from V_{SS} + 2 to V_{CC} – 2 V. 1-Hz to 10-kHz voltage noise of 7-3-1.5-1.2-1.1 nV/√Hz. Current noise 11 pA (1 Hz)- 4.5-2.9-2.7-2.7. Supply 4.5 to 36 V. Input bias 60 to 350 nA. 40- to 80-MHz GBW.	Single $1.75 @ 1k Dual $2.75 @ 1k Outstanding noise performance, current noise is about 5X the OPA209, but much lower than competing MAX9632. The OPA211 is a more expensive version with better input voltage limits.
TI LMP7731 (single) and LMP7732 (dual)	Rail-to-rail input and output. Voltage noise 4.2 (1 Hz)-3.1-3.0-2.9 nV. Current noise 8 pA (1 Hz)-3-1.2-1.1 pA. Supply 1.8 to 5.5 V, input bias 1.5 to 5 0nA. 22-MHz GBW.	Single $0.63 @ 1k Dual $1.05 @ 1k Lowest noise RRIO part from TI. The competing Linear LT1678 dual RRIO has noise of 7.5 (1 Hz)-4.5-4.0-3.9 nV.
Linear LT1677	Among lowest-noise RRIO op amps with higher voltage. Voltage noise 18 (1 Hz)-5.2-3.3-3.2 nV. Current noise 1.2 pA (10 Hz)-0.4-0.3. 3- to ±18-V supply, ~3 mA 7.2-MHz GBW.	~$2.80 @ 1000 distributor. LT1678 is a similar dual version, ~$3.15 @ 1000 distributor. Suitable for low-noise (not ultra-low noise) single op-amp loop filters where its rail-to-rail performance simplifies circuit design of locking problems that unassisted non-RR op amps may suffer.
TI OPA2156	Dual low-cost, low-noise, high-voltage RR op amp. Voltage noise 150 (1 Hz)-40-11-4-2.9 nV. Current noise 19 fA at 1 kHz. 4.5- to 36-V supply, ~4.4 mA. 25-MHz GBW.	First of a new family, single op-amp versions likely to follow. Dual: $1.25 @ 1k. High 1/f corner ~700 Hz, but this can be suppressed by a wideband synthesizer. Suitable for single op-amp loop filter with op amp to spare.
TI LM7321 LM7322	RR input and output. Noise 100 (1 Hz)-40-18-15 nV. 2.5- to 32-V supply, 1.3 mA. 20-MHz GBW.	Single: $0.71 @ 1k Dual: $0.97 @ 1k Suitable as a rail-to-rail op amp for settling the active filter prior to switching in an ultra-low-noise non-RR op amp.

Listed are low-noise op amps for use in low-noise synthesizers. The shorthand W-X-Y-Z here refers to spectral noise density (voltage or current) at frequencies spaced a decade apart, usually starting at 1 Hz.

JOEL BRAND | Vice President, Product Management at Kumu Networks
www.kumunetworks.com

The Rise and Fall of IoT in the 2.4-GHz Band

Self-interference cancellation could very well be the linchpin to a resurgence of the 2.4-GHz band.

Way back when the 5-GHz band was opened for unlicensed Wi-Fi usage, many predicted the death of 2.4 GHz. The 5-GHz band enabled much faster speeds thanks to the increased amount of bandwidth available at the higher frequency. Channels as wide as 160 MHz were introduced (and the industry is mulling the introduction of 320-MHz channels), whereas the entire 2.4-GHz band is only about 80 MHz wide.

As the FCC and other regulators are looking to open the 6-GHz band for Wi-Fi usage, there's no doubt that consumer appetite for higher bandwidth and faster speed will be served at the higher frequencies. However, Internet of Things (IoT) devices don't care about bandwidth.

With relatively little information to transfer, power consumption is their prime consideration. After all, the labor costs associated with battery replacement of millions and billions of IoT devices installed on every imaginable product is prohibitive.

To conserve power and prolong battery life, active sensors attempt to reduce the time in which they transmit, as their power amplifier is consuming more power than anything else in the system. They also reduce the transmission power as the power consumption increases with the output power of the radio.

Thus, IoT networks prefer lower frequencies that propagate further. They typically rely on mesh architectures to ensure that transmissions need to reach a fairly nearby receiver—the next hop in the mesh. And they absolutely prefer to avoid unnecessary retransmissions as these accelerate the battery drainage.

RETRANSMISSIONS AND INTERFERENCE

Why would an IoT device need to retransmit? It would need to retransmit if a sent packet doesn't reach its destination. If this happens because the destination is too far away, this is simply a poor design of the network. More likely, packets would get lost due to interference.

The 2.4-GHz band is extremely crowded with Wi-Fi access points and other devices emitting energy *(Fig. 1)*. Yet, frequency-hopping techniques, channel selection, modulations, waveforms, error correction at the protocol level, and other mechanisms are designed to counter the effect of inter-

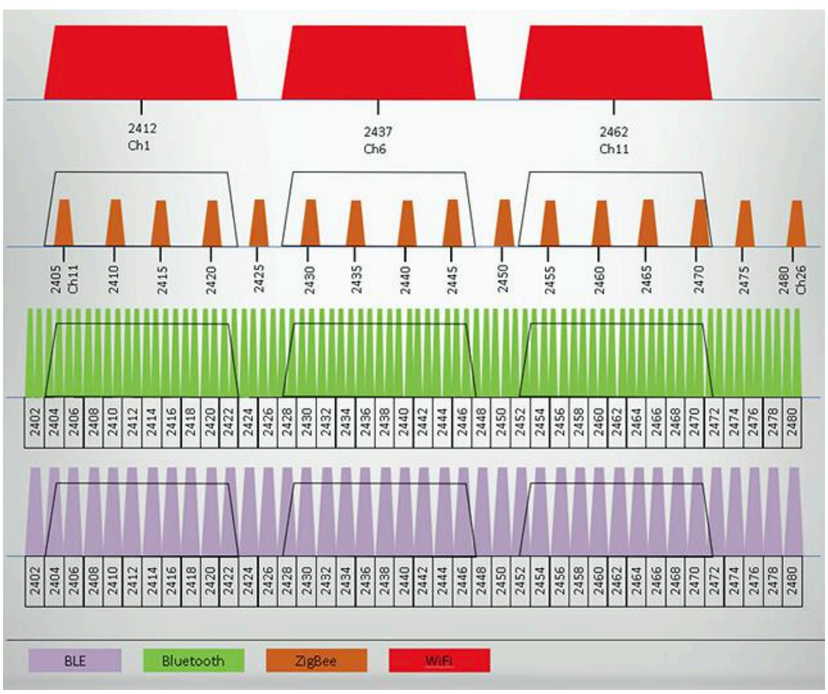

1. The 2.4-GHz band is extremely crowded with Wi-Fi access points, Bluetooth, and other devices emitting energy.

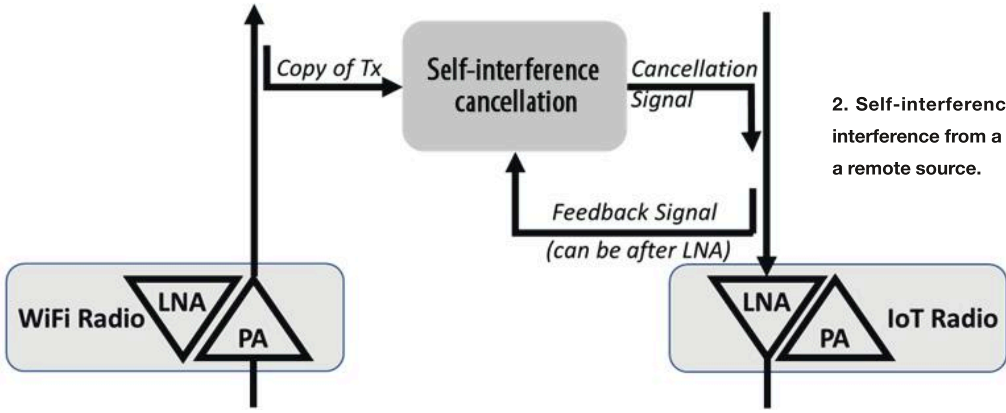

2. Self-interference cancellation eliminates interference from a local source as opposed to a remote source.

ference. Nevertheless, none of these techniques would help if the interferer is too strong.

Regulators impose restrictions on maximum power levels that a device can emit at the unlicensed (ISM) bands. This is done exactly to avoid the monopolization of the spectrum by a single device (and to ensure that the device doesn't fry us humans). So external interference, while it certainly exists and has the potential to be harmful, is exactly what IoT devices are designed to avoid.

But what happens when the receiver (typically an IoT hub of some sort) is blasted with energy right in its antenna? This would be the equivalent of you screaming while trying to listen to a whisper coming from afar—you would not be able to hear the whisper. But why would someone "scream" in the "ears" of the IoT hub? IoT hubs may be standalone devices, but more likely they would be integrated into Wi-Fi access points to avoid the need for separate wiring.

BLE, ZIGBEE, ETC.

Check the market. All major enterprise Wi-Fi vendors have BLE (Bluetooth Low Energy) receivers integrated into their product portfolio. And all major service providers are rolling out Wi-Fi access points that incorporate IoT receivers in the form of BLE or Zigbee radios. This is also true for consumer solutions from the likes of Google Wi-Fi.

Yes, when the 2.4-GHz Wi-Fi radio transmits, the IoT receiver is saturated. It doesn't matter that the IoT radio operates on a different channel or that it applies any and all of the other interference avoidance techniques. It's saturated. Period. Any incoming transmission would get lost and the originating IoT device would have to retransmit it. Is this a problem? Maybe not if you have one water sensor under the dishwater. But if IoT is truly to take off, at home, in the enterprise, and in what's termed the Industrial IoT, this would be a serious problem.

In fact, the interference between Wi-Fi and Bluetooth is already a serious problem. Today, it's most noticeable when Wi-Fi- and Bluetooth-based audio streaming are trying to co-exist. Unknowingly to you, the user, Wi-Fi 2.4 GHz is throttled to the absolute minimal throughput when a co-located Bluetooth receiver is used. And this is likely to be a growing problem as personal assistant devices would double up as Wi-Fi extenders, or when Wi-Fi access points would be more pervasive in cars where the driver heavily relies on Bluetooth audio streaming to comply with the 'no hands' laws.

SELF-INTERFERENCE CANCELLATION

There is a solution. It's called self-interference cancellation. The "self" denotes that the interference comes from a local source as opposed to a remote source. This is important because the self-interference cancellation technique is based on an exact copy of the interfering signal, which can easily be provided if we could connect a local wire to it. The system "subtracts" this interferer from the signal incoming into the interfered receiver to ensure that only a clean desired signal makes its way into the receiver *(Fig. 2)*.

It's not as simple as that because interference has the nasty habit of changing when someone places a transmitter in front of a reflecting metal cabinet or a refrigerator. In other words, the interference, even if it's local, is affected by the environment. Kumu Networks has developed self-interference cancellation that's designed to adapt to the environment and "cancel" or "subtract" the interfering noise from the desired signal. This allows Wi-Fi, Bluetooth, Zigbee, and other protocols to coexist in the same very narrow 2.4-GHz band, even if these radios are co-located in the same enclosure. mw

FOR OVER 25 YEARS, Joel Brand has actively participated in defining and building infrastructure solutions for the telecom and wireless industries. He previously held executive positions at ConteXtream (acquired by HP), Bytemobile (acquired by Citrix), and Ruckus Wireless (NYSE: RKUS and now part of Arris). Joel holds a B.Sc. and M.Sc. in Engineering from the Israeli Institute of Technology (the Technion) as well as an MBA from National University in San Diego.

CHRIS DeMARTINO | Editor

Analyze Multiple Domains with Just One Oscilloscope

Equipped with new mixed-domain analysis capability, this scope goes above and beyond traditional measurements.

When discussing oscilloscopes, Tektronix *(www.tek.com)* is a name that will likely come up thanks to the company's long history with this ubiquitous test instrument. While Tektronix has been in the business of manufacturing oscilloscopes for many years, the company continues to push the technology bar higher with its latest products and innovations.

For example, last year, I wrote about Tektronix's 6 Series MSO Oscilloscopes, which were introduced right about that time. The 6 Series MSO instruments offer a bandwidth as high as 8 GHz along with 25-Gsample/s sample rates.

Here, I'll present a closer look at the 6 Series MSO oscilloscopes, since Tektronix was kind enough to loan me one *(Fig. 1)*. Specifically, this article explores a significant feature known as Spectrum View, which brings mixed-domain analysis to the 4, 5, and 6 Series MSO oscilloscopes. Spectrum View makes it possible to not only perform time- and frequency-domain analysis at the same time, but independently optimize displays of both domains. That means changing the measurement settings in one domain has no effect on the other.

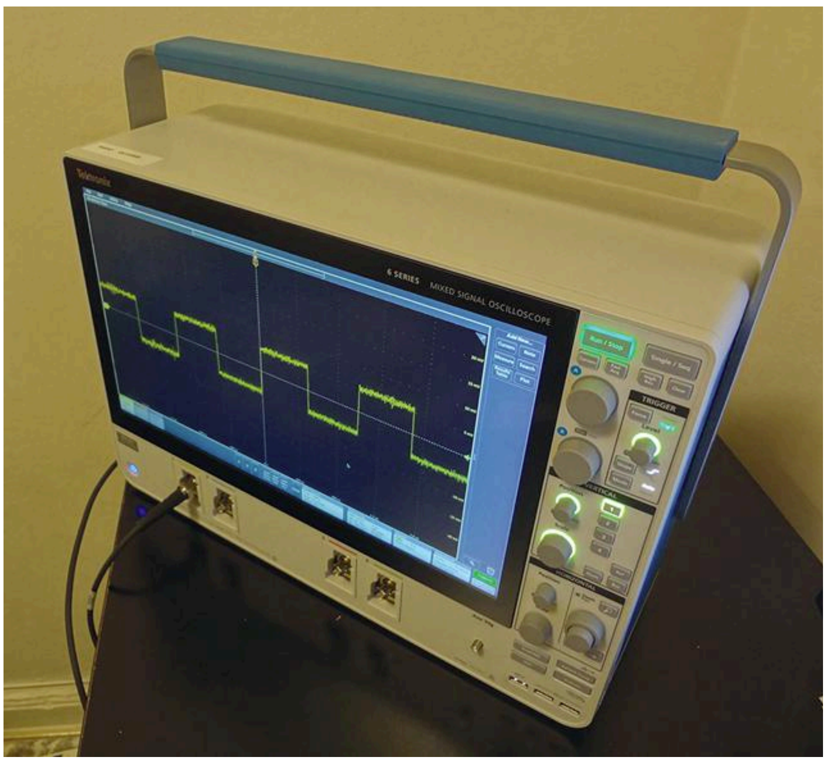

1. Here's the 6 Series MSO oscilloscope featured in this article.

A QUICK INTRODUCTION

First, let's take a quick general look at the 6 Series MSO oscilloscope. When using one of these instruments, one can't help but notice the aesthetic 15.6-in. display. A significant aspect of these instruments is touchscreen operation, which will likely appeal to those who are accustomed to using smartphones and tablets (i.e., most anyone reading this article). Of course, the familiar knobs and buttons can still be used. Furthermore, those who may not be in favor of touchscreen operation can connect a mouse and/or keyboard to a 6 Series MSO oscilloscope as an alternative means of operating the instrument.

The oscilloscopes come equipped with various triggering techniques. Among them are *Edge, Pulse Width, Timeout, Runt, Window, Logic, Setup & Hold, Rise/Fall Time, Bus,* and *Sequence*. The 6 Series MSO oscilloscopes also feature visual triggering, which enables users to build complex waveform triggers by simply drawing shapes using the touchscreen or a mouse.

Another aspect worth mentioning is the optional integrated arbitrary function generator (AFG), which, according to Tektronix, is ideal for simulating sensor signals within a design or adding noise to signals to perform margin testing. The AFG provides various predefined waveforms at frequencies as high as 50 MHz. Waveform types include *Sine, Square, Pulse, Ramp, DC, Noise, Sin(x)/x, Gaussian, Lorentz*, and more. Furthermore, the AFG can load waveform records from an internal file location or a USB mass-storage device. The AFG feature is compatible with Tektronix's ArbExpress PC-based waveform creation and editing software.

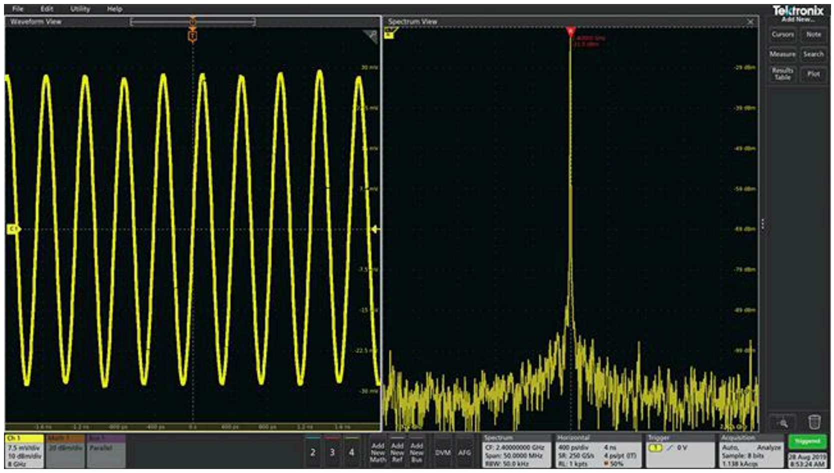

2. Shown is a time-domain waveform of a 2.4-GHz CW signal along with the Spectrum View display.

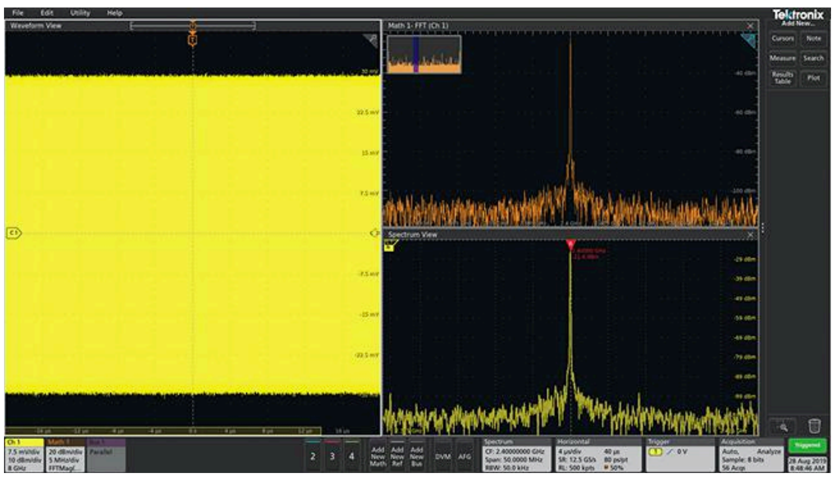

3. These three displays are the time-domain waveform, the FFT display, and the Spectrum View display.

FREQUENCY-DOMAIN ANALYSIS WITH SPECTRUM VIEW

Tektronix introduced the Spectrum View feature earlier this year. For those already using the 5 and 6 Series MSO oscilloscopes, simply upgrading the firmware enabled access to Spectrum View. Of course, Spectrum View is included right out of the box for new 5 and 6 Series MSO oscilloscopes, and it's also an optional feature for the new 4 Series MSO instruments.

Once again, the Spectrum View analysis tool makes it possible to simultaneously view time- and frequency-domain displays. Tektronix speaks very highly of Spectrum View, stating that it represents "a new approach to frequency-domain analysis on oscilloscopes." But how does Spectrum View measure up? To answer that question, let's see it in action.

Figure 2 shows the time-domain waveform of a 2.4-GHz continuous-wave (CW) signal with the horizontal scale set to 400 ps/div. Also shown is the corresponding Spectrum View display. For myself, using Spectrum View basically felt like operating a spectrum analyzer inside of an oscilloscope. That's because Spectrum View features the same controls you would find on a spectrum analyzer, such as center frequency, span, and resolution bandwidth (RBW).

Consequently, anyone who has used a spectrum analyzer should not have a problem using Spectrum View. In *Figure 2,* the center frequency, span, and RBW are set to 2.4 GHz, 50 MHz, and 50 kHz, respectively.

Some may question how Spectrum View could possibly represent "a *new* approach to frequency-domain analysis on oscilloscopes," since oscilloscopes have long offered frequency-domain analysis via fast-Fourier-transform (FFT) measurements. However, according to Tektronix, Spectrum View holds a significant advantage over traditional FFT measurements: Time- and frequency-domain measurement displays can be optimized independently, as mentioned earlier. Let's look at this more closely by using the 6 Series MSO oscilloscope to compare a Spectrum View measurement with a traditional FFT measurement.

Figure 3 depicts an analysis of the same 2.4-GHz CW signal. Here, the time-domain waveform is shown on the left, but the horizontal scale has been changed from 400 ps/div to 4 µs/div. *Figure 3* also shows the FFT view on the top right, while the Spectrum View display can be seen on the bottom right. It's clear that with the horizontal scale set to 4 µs/div, the Spectrum View and FFT displays are nearly identical.

Now, let's change the horizontal scale back to 400 ps/div. *Figure 4* shows the same three displays, but this time with the horizontal scale once again set to 400 ps/div. It's clear from *Figure 4* that changing the horizontal scale affected the FFT display because the same acquisition drives the time-domain and FFT

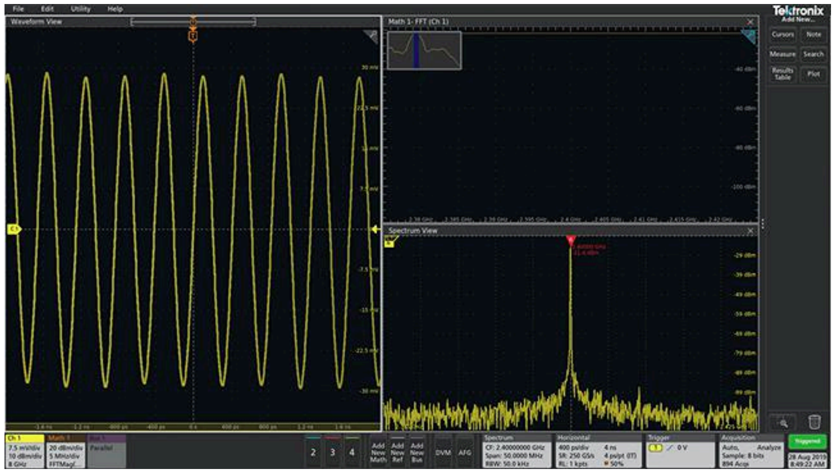

4. After changing the horizontal scale to 400 ps/div, the FFT display is no longer effective.

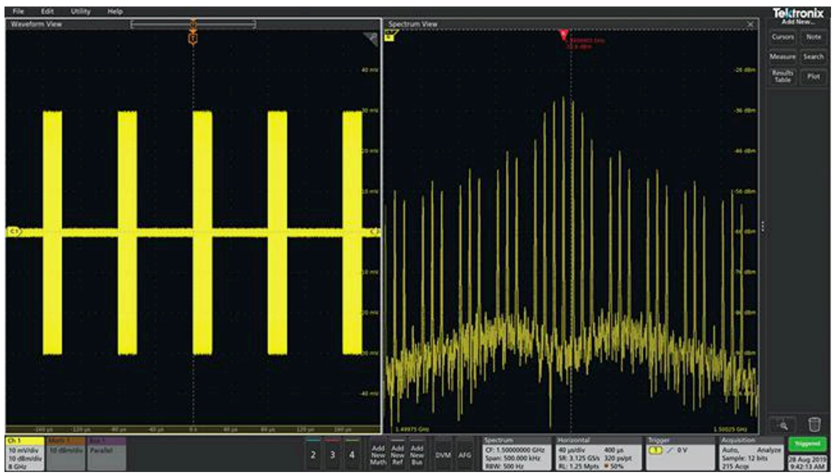

5. Shown is a pulsed RF analysis in both the time and frequency domains.

measurements. Unfortunately, the FFT display has obviously lost its usefulness, since it now takes the form of a straight line. This demonstrates that adjusting the horizontal scale to achieve a specific time-domain display can essentially render useless the FFT display. The opposite is also true—adjusting the settings to achieve a desired FFT view can have an adverse effect on the time-domain view.

In contrast, *Figure 4* also revealed that changing the horizontal scale had no effect on the Spectrum View display, demonstrating how time-domain waveform views can be optimized without affecting the Spectrum View display. In the same manner, adjusting the Spectrum View display would have no effect on the waveform view. This simple demonstration helps illustrate the effectiveness of the Spectrum View analysis tool.

Of course, the benefits of using Spectrum View extend far beyond CW signals. Users can take advantage of Spectrum View by performing mixed-domain analysis for more complex use cases like pulsed RF signals, which they may want to analyze in both the time and frequency domains.

As a quick example, utilizing the trigger holdoff function, *Figure 5* shows the time-domain waveform of a pulsed RF signal along with the corresponding Spectrum View display. Here, the horizontal scale is set to 40 µs/div. *Figure 6* shows the same measurement, but with the horizontal scale now set to 2 ns/div. Of course, the Spectrum View display remained unchanged like in the previous demonstration.

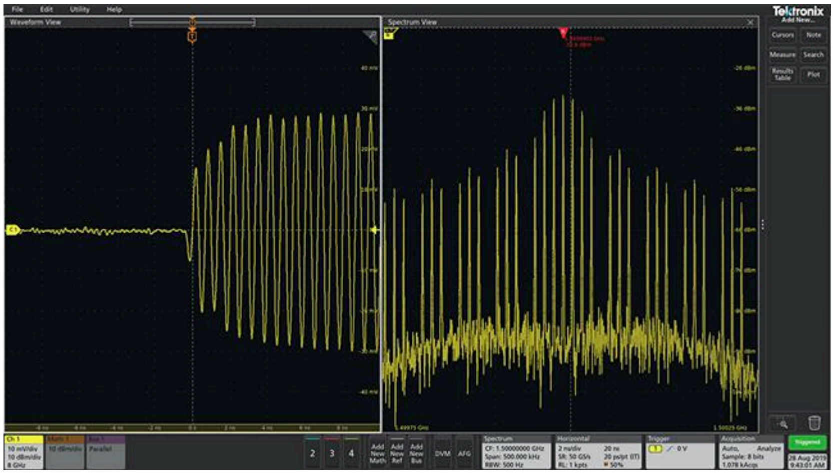

6. The horizontal scale was changed to 2 ns/div, but the Spectrum View display remained the same.

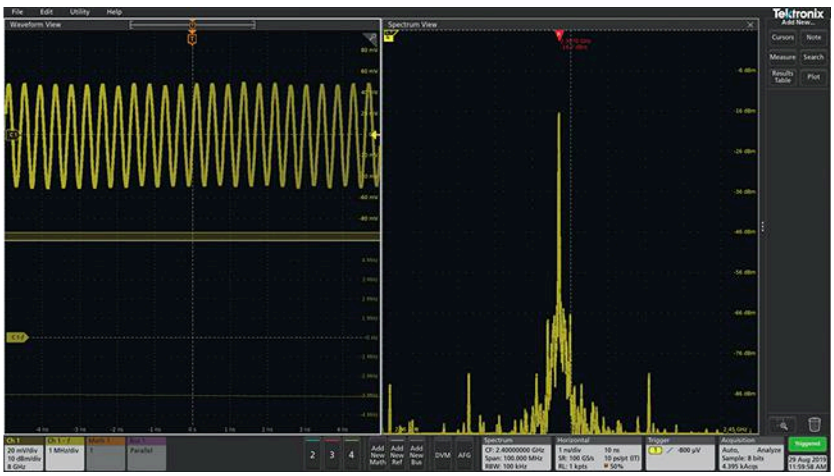

7. The frequency-versus-time measurement (bottom left) reveals that the carrier frequency is below the 2.4-GHz center frequency.

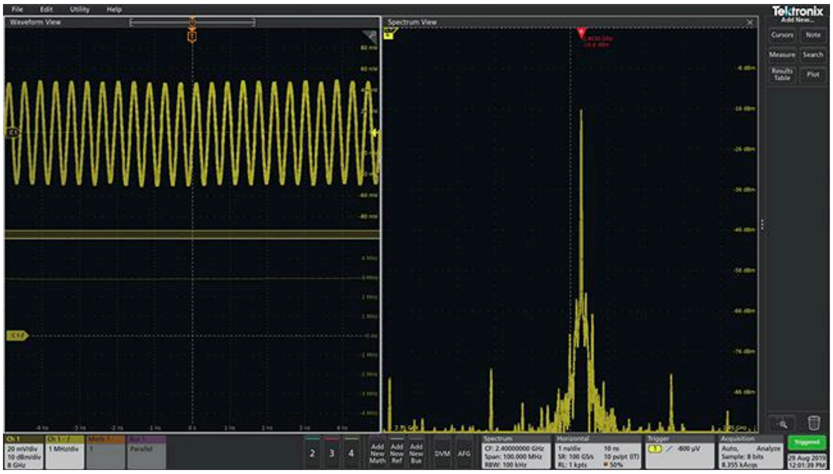

8. The carrier frequency is above the 2.4-GHz center frequency, as can be seen from the frequency-versus-time measurement (and the Spectrum View display).

RF VERSUS TIME AND FINAL THOUGHTS

One feature that was recently added to the 6 Series MSO Oscilloscopes is RF-versus-time capability. Thanks to this feature, when measuring RF signals, it's possible to measure three parameters over time: magnitude, frequency, and phase.

Figures 7 and 8 demonstrate a frequency-versus-time measurement. In this case, a frequency-hopping scenario was measured—a signal that was centered at 2.4 GHz stepped up and down by 3 MHz. Both figures show the frequency-versus-time measurement on the bottom left. The figures also depict the time-domain waveforms and Spectrum View displays. In *Figure 7,* the carrier frequency has stepped below the 2.4-GHz center frequency, while *Figure 8* shows the carrier frequency above the center frequency.

In closing, there's not much to dislike about the 6 Series MSO oscilloscopes. The instruments offer a pleasing user interface with all of the performance and features one could ask for in an oscilloscope. And by adding Spectrum View to the mix, it appears that Tektronix has accomplished its goal of creating a new approach to frequency-domain analysis with an oscilloscope. Whatever test needs are being sought, Tektronix's latest innovations may be just what the doctor ordered. mw

Coaxial Amplifier Powers 600 to 6000 MHz

MINI-CIRCUITS' MODEL ZHL-5W-63-S+ is a coaxial Class AB linear amplifier with high gain and medium output power from 0.6 to 6.0 GHz. It delivers typical gain of 45 dB with gain flatness of ±3.5 dB across the full frequency range. The RoHS-compliant, GaN-based amplifier provides +35-dBm output power at 3-dB compression and +37-dBm saturated output power. It has a typical output third-order intercept point (OIP3) of +42 dBm. The noise performance is consistent across the wide bandwidth, with a typical noise figure of 12 dB. Typical input VSWR is 2.50:1, while typical output VSWR is 3.50:1. Suitable for mobile communications, satellite communications (satcom), and test-and-measurement applications, the 50-Ω amplifier comes in a compact aluminum housing with female SMA connectors. It measures 7.25 × 4.33 × 3.34 in. (184.15 × 109.98 × 84.836 mm) excluding the connectors or optional heatsink, and draws 3 A typical current from a +28-V dc supply. It's designed to handle input power as high as +7 dBm without damage and has an operating temperature range of 0 to +60°C.

MINI-CIRCUITS, P.O. Box 350166, Brooklyn, NY 11235-0003; (718) 934-4500,
https://www.minicircuits.com/WebStore/dashboard.html?model=ZHL-5W-63-S%2B

Designer's Kit Features 100 2.4- and 5-GHz Filters

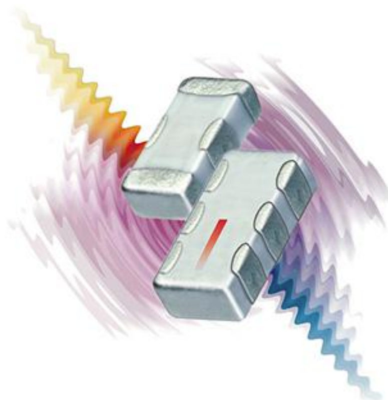

THE K1-LTCC-WBZ+ DESIGNER'S KIT from Mini-Circuits is a comprehensive collection of lowpass, highpass, and bandpass filters, diplexers, and balanced filters (baluns) well-suited for Wi-Fi, Bluetooth, and Zigbee applications in the 2.4- and 5-GHz bands. Based on low-temperature co-fired-ceramic (LTCC) construction, the assortment contains five each of 20 different models for a total of 100 filtering components covering the two frequency ranges. As an example, model LPGE-252R+ is a lowpass filter with low typical insertion loss of only 0.3 dB across its 2.4- to 2.5-GHz passband. It has three stopbands each with high rejection: 44 dB from 4.8 to 5.0 GHz, 40 dB from 7.2 to 7.5 GHz, and 37 dB from 9.6 to 10.0 GHz. At higher frequencies, model BPNK-542R+ is a bandpass filter with just 1.0-dB typical insertion loss across its 4.9- to 5.9-GHz passband. It provides 40-dB typical rejection of unwanted signals from dc to 2.7 GHz and 34-dB rejection from 9.8 to 12.0 GHz. All of the filters in the kit are RoHS-compliant. The rugged devices are designed to handle power levels as high as 2 W (+33 dBm).

MINI-CIRCUITS, P.O. Box 350166, Brooklyn, NY 11235-0003; (718) 934-4500,
https://www.minicircuits.com/WebStore/dashboard.html?model=K1-LTCC-WBZ%2B

Linear Amp Holds Gain Flat from 26 to 40 GHz

MINI-CIRCUITS' ZVE-403-K+ is a compact Class A linear amplifier with a broad frequency range of 26 to 40 GHz. It offers 22-dB typical gain across the full bandwidth, with typical gain flatness of ±2 dB. The four-stage amplifier delivers +19-dBm typical output power at 1-dB compression and +21-dBm typical output power at 3-dB compression, with typical output third-order intercept (OIP3) of +28 dBm. The 50-Ω amplifier exhibits typical input and output VSWR of 2.0:1, with typical noise figure of 9 dB. It can operate with supply voltages ranging from 11 to 14 V dc, drawing 300 mA typical current from a 12-V dc supply. The unconditionally stable, RoHS-compliant amplifier is equipped with K-type (2.92-mm) coaxial connectors. The amplifier is supplied in a rugged housing measuring 1.2 × 0.46 × 0.45 in. (30.48 × 11.58 × 11.43 mm), not including the connectors or an optional heat sink. It's designed for an operating temperature range of –40 to +60°C.

MINI-CIRCUITS, P.O. Box 350166, Brooklyn, NY 11235-0003; (718) 934-4500,
https://www.minicircuits.com/WebStore/dashboard.html?model=ZVE-403-K%2B

Faraday Isolator Covers 140 to 220 GHz

MODEL STF-05-S1-C is a Faraday isolator that operates from 140 to 220 GHz. It's constructed with a longitudinal, magnetized ferrite rod that causes a Faraday rotation of the incoming RF signal. The compact, robust package makes the STF-05-S1-C well-suited for system integration and testing applications. The device achieves a typical isolation of 30 dB along with 5.0 dB of nominal insertion loss. For the input and output ports, the STF-05-S1-C is built with WR5 waveguide connectors featuring UG-387/U-M flanges.

SAGE MILLIMETER, 3043 Kashiwa Street, Torrance, CA 90505; (424) 757-0168, www.sagemillimeter.com

Packaged GaAs Amplifier Spans dc to 40 GHz

THE CMD242K4 is a wideband GaAs MMIC distributed low-noise amplifier that operates from dc to 40 GHz. Housed in a leadless surface-mount package, the amplifier delivers more than 10.5 dB of gain at 20 GHz. At the same frequency, the CMD242K4 achieves a noise figure of 5 dB and delivers +17.5 dBm of output power at 1-dB compression. With a drain voltage of +8.0 V dc and a gate voltage of –0.32 V dc, typical supply current is 100 mA. The CMD242K4 is designed for an operating temperature range of –40 to +85°C.

CUSTOM MMIC, 300 Apollo Dr., Chelmsford, MA 01824; (978) 467-4290, www.custommmic.com

United States Postal Service

Statement of Ownership, Management, and Circulation **(Requester Publications Only)**

1. Publication Title: Microwaves & RF
2. Publication Number: 797-680
3. Filing Date: 8/28/19
4. Issue of Frequency: Monthly
5. Number of Issues Published Annually: 12
6. Annual Subscription Price: Free to Qualified
7. Complete Mailing Address of Known Office of Publication (Not Printer): Informa Media, Inc., 9800 Metcalf Ave., Overland Park, Johnson County, KS 66212-2216 — Contact Person: Debbie Brady, Telephone: 216-931-9882
8. Complete Mailing Address of Headquarters or General Business Office of Publisher (Not Printer): Informa Media, Inc.,605 Third Ave, New York, NY 10158
9. Full Names and Complete Mailing Addresses of Publisher, Editor, and Managing Editor - Publisher: Paul Miller, Informa Media, Inc., 605 Third Ave, New York, NY 10158; Editor: Karen Field, Informa Media, Inc., 605 Third Ave, New York, NY 10158; Managing Editor: ,
10. Owner - Full name and complete mailing address: Informa Media, Inc., 605 Third Ave, New York, NY 10158; Informa Operating Holdings, Inc. (owns 100% of the stock of Informa Media, Inc.), 605 Third Ave, New York, NY 10158
11. Known Bondholders, Mortgagees, and Other Security Holders Owning or Holding 1 Percent or More of Total Amount of Bonds, Mortgages or Other Securities: None
12. Tax Status (For completion by nonprofit organizations authorized to mail at nonprofit rates) (Check one) The purpose, function, and nonprofit status of this organization and the exempt status for federal income tax purposes: N/A
13. Publication Title: Microwaves & RF

14. Issue Date for Circulation Data: August 2019 15. Extent and Nature of Circulation	Average No. Copies Each Issue During Preceding 12 Months	No. Copies of Single Issue Published Nearest to Filing Date
a. Total Number of Copies (Net press run)	33,842	33,263
b. Legitimate Paid and/or Requested Distribution (By Mail and Outside the Mail)		
(1) Outside County Paid/Requested Mail Subscriptions stated on PS Form 3541. (Include direct written request from recipient, telemarketing and Internet requests from recipient, paid subscriptions including nominal rate subscriptions, employer requests, advertiser's proof copies, and exchange copies.)	25,347	24,697
(2) In-County Paid/Requested Mail Subscriptions stated on PS Form 3541. (Include direct written request from recipient, telemarketing and Internet requests from recipient, paid subscriptions including nominal rate subscriptions, employer requests, advertiser's proof copies, and exchange copies.)	0	0
(3) Sales Through Dealers and Carriers, Street Vendors, Counter Sales, and Other Paid or Requested Distribution Outside USPS®	6,692	6,395
(4) Requested Copies Distributed by Other Mail Classes Through the USPS (e.g. First-Class Mail®)	0	0
c. Total Paid and/or Requested Distribution (Sum of 15b (1), (2), (3), and (4))	32,039	31,092
d. Nonrequested Distribution (By Mail and Outside the Mail)		
(1) Outside County Nonrequested Copies Stated on PS Form 3541 (include Sample copies, Requests Over 3 years old, Requests induced by a Premium, Bulk Sales and Requests including Association Requests, Names obtained from Business Directories, Lists, and other sources)	726	786
(2) In-County Nonrequested Copies Stated on PS Form 3541 (include Sample copies, Requests Over 3 years old, Requests induced by a Premium, Bulk Sales and Requests including Association Requests, Names obtained from Business Directories, Lists, and other sources)	0	0
(3) Nonrequested Copies Distributed Through the USPS by Other Classes of Mail (e.g. First-Class Mail, Nonrequestor Copies mailed in excess of 10% Limit mailed at Standard Mail® or Package Services Rates)	0	0
(4) Nonrequested Copies Distributed Outside the Mail (Include Pickup Stands, Trade Shows, Showrooms and Other Sources)	129	200
e. Total Nonrequested Distribution (Sum of 15d (1), (2), (3), and (4))	855	986
f. Total Distribution (Sum of 15c and 15e)	32,893	32,078
g. Copies not Distributed	948	1,185
h. Total (Sum of 15f and g)	33,842	33,263
i. Percent Paid and/or Requested Circulation (15c divided by 15f times 100)	97.40%	96.93%
16 Electronic Copy Circulation		
a. Requested and Paid Electronic Copies	-	-
b. Total Requested and Paid Print Copies (Line 15c)+ Requested/Paid Electronic Copies (Line 16a)	32,039	31,092
c. Total Requested Copy Distribution Distribution(Line 15f) + Requested/Paid Electronic Copies (Line 16a)	32,893	32,078
d. Percent Paid an/dor Requested Circulaltion (Both Print & Electronic Copies) (16b diveded by 16c x 100)	97.40%	96.93%

[X] I certify that 50% of all my distribution copies (electronic and print) are legitimate requests or paid copies:

17. Publication of Statement of Ownership for a Requester Publication is required and will be printed in the: Oct-19 issue of this publication.

18. Debbie Brady, Manager, User Marketing — Date 8/28/19

I certify that all information furnished on this form is true and complete. I understand that anyone who furnishes false or misleading information on this form or who omits material or information requested on the form may be subject to criminal sanctions (including fines and imprisonment) and/or civil sanctions (including civil penalties).

PS Form 3526-R, July 2014

This index is provided as an additional service by the publisher, who assumes no responsibility for errors or omissions.

Subscription Assistance and Information:
(ISSN 0745-2993)

Microwaves & RF is published monthly. Microwaves & RF is sent free to individuals actively engaged in high-frequency electronics engineering. In addition, paid subscriptions are available. Subscription rates for U.S. are $95 for 1 year ($120 in Canada, $150 for International). Published by Informa Media Inc., 9800 Metcalf Ave., Overland Park, KS 66212-2216. Periodicals Postage Paid at Kansas City, MO and additional mailing offices.

POSTMASTER: Send change of address to Microwaves & RF, PO Box 2100, Skokie, IL 60076-7800. For paid subscription information, please contact Microwaves & RF at PO Box 2100, Skokie IL 60076-7800. Canadian GST #R126431964.

Back issues of MicroWaves and Microwaves & RF are available on microfilm and can be purchased from National Archive Publishing Company (NAPC). For more information, call NAPC at 734-302-6500 or 800-420-NAPC (6272) x 6578. Copying: Permission is granted to users registered with the Copyright Clearance Center, Inc. (CCC) to photocopy any article, with the exception of those for which separate copyright ownership is indicated on the first page of the article, provided that a base fee of $1.25 per copy of the article plus 60 cents per page is paid directly to the CCC, 222 Rosewood Dr., Danvers, MA 01923. (Code 0745–2993/02 $1.25 +.60) Copying done for other than personal or internal reference use without the expressed permission of Informa Media Inc., is prohibited. Requests for special permission or bulk orders should be addressed in writing to the publisher.

Ultra high bandwidth Payload & RF Multipath Link Emulator

Just released ...

Sophisticated high bandwidth (up to 600MHz) emulation of physical layer RF link effects channel modeling (delay, Doppler, AWGN, Multipath) and hardware in the loop impairments modeling (programmable Group delay, Phase noise, gain/compression distortion and non-linearity AM/AM, AM/PM simulation etc.

Comprehensive range of instruments from 72 MHz to 600 MHz bandwidth with a wide RF frequency tuning range.

Contact dBm for specifications, pricing information and demonstration/evaluation units.

- **RF physical layer Link emulation**
- **Point to Point UHF/VHF radio testing**
- **Real time control for Arial Vehicle (UAV) testing**
- **Payload and ground station emulation**
- **Multipath, 12 paths @ 600MHz BW**

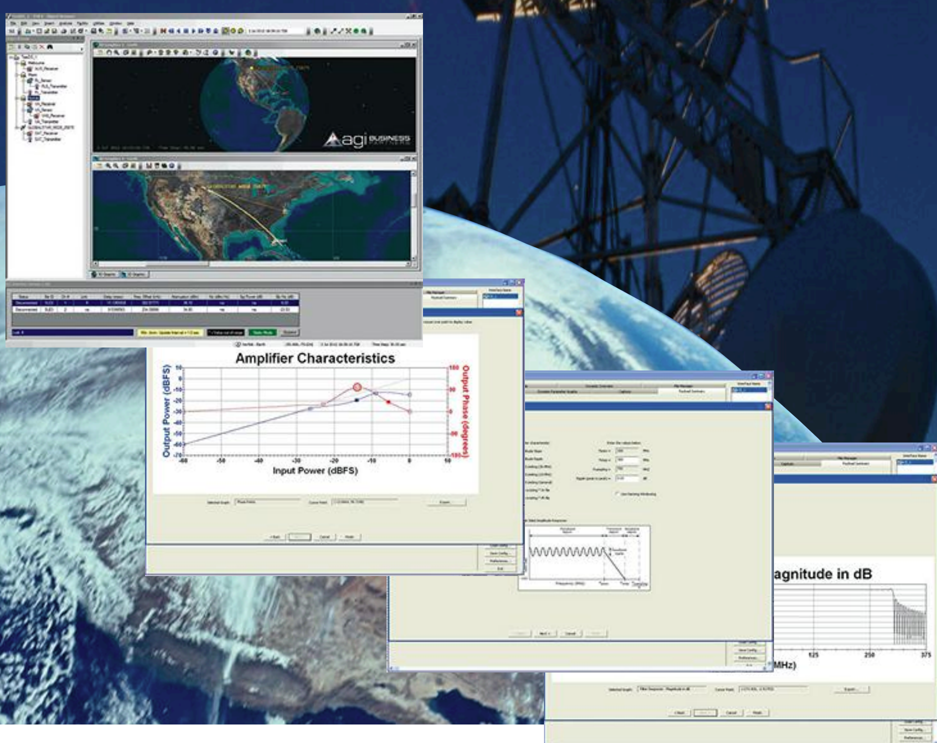

dBm

RF Test Equipment for Wireless Communications

email: info@dbmcorp.com

dBm Corp, Inc
32A Spruce Street ◆ Oakland, NJ 07436
Tel (201) 677-0008 ◆ Fax (201) 677-9444
www.dbmcorp.com